A symmetric planar waveguide chip for fluorescence microscopy

Nina B. Arnfinnsdottir

60 ECTS thesis submitted in partial fulfillment of a
Magister Scientiarum degree in Physics

Advisors
Dr. Kristján Leósson
Dr. Þórarinn Guðjónsson

External examiner
Hans G. Þormar, M.Sc.

Faculty of Physical Sciences
School of Engineering and Natural Sciences
University of Iceland
Reykjavík, May 2010

Abstract

The fluorescence imaging properties of a planar symmetric waveguide chip where the cladding layer is index matched to that of biological samples are investigated. A well in the top cladding layer of the waveguide accommodates for a biological sample, and light that propagates in the waveguide layer will penetrate a short distance into the sample. This penetrating evanescent wave can excite fluorophores in the sample, and the chip can be used for fluorescence imaging.

The chip is tested for fluorescence imaging of both fixed and living cells. Cells from the cell line MCF7 are used for fluorescence imaging of fixated cells on the chip. For live cell imaging, LLC PK1 cells that stably express GFP are used. Procedures for culturing cells on the chip are described in detail, along with the imaging set up. Images obtained are presented, and the evanescent wave exitation microscopy technique is compared to traditional epi-fluorescence imaging.

Contents

Acknowledgements

I would like to thank my supervisor Dr. Kristjan Leosson for his guidance through out my work on this thesis.

I would also like to thank Jen Halldorsson and Björn Agnarsson, along with the rest if the group, for help with experiments and always being willing to lend a hand. I would like to thank Asta B. Jonsdottir and Saevar Ingthorson for teaching me how to culture cells.

Last, but not least, I would like to thank Jen for all of the lovely cakes she has made during my work on this thesis.

1 Introduction

Fluorescence microscopy is the most rapidly expanding microscopy technique today. The use of fluorescent markers for identification of cells and sub-microscopic cellular components has made it an essential tool in biology and the biomedical sciences[Nikon Instruments, 2010a].

The use of evanescent wave excitation, like in a Total Internal Reflection Fluorescence (TIRF) microscope, has become a very important characterization technique for events in the regions near the cell membrane. In a TIRF microscope, total internal reflection at a glass to sample boundary generates a evanescent field that typically penetrates up to 100 nm into the sample[Nikon Instruments, 2010a]. The short penetration depth gives very low background fluorescence by eliminating excitation of fluorophores in the out-of-focus areas. This improves image quality and enables the TIRF microscope to perform selective visualization of cell-to-substrate contact regions and even visualization of single fluorescent molecules[Axelrod, 2001].

Evanescent wave microscopy can also be accomplished with planar waveguides structures. Light propagating in the waveguide will penetrate into the cladding material, and by having biological samples with fluorescent molecules as part of the cladding material, the penetrating evanescent field will excite fluorophores within the sample. The penetration depth depends on the waveguide geometry, refractive indexes of both the core and cladding materials and the wavelength and polarization of the propagating light.

Evanescent wave fluorescence microscopy has been reported for waveguides with $Si_xTi_{1-x}O_2$ or Ta_2O_5 waveguiding films on a glass substrateGrandin et al. [2006]. These mono mode waveguides have a penetration depth in the order of 100 to 200 nm, and laser light is coupled into the waveguiding layer through a sub micron grating pattern at a wavelength-dependent angle. Fixed cell imaging have been performed on such waveguides, but imperfections in the grating patterns limited the imaging quality of the waveguide.

To increase the range of penetration depths, reversed symmetry waveguides have been reported [Horvath et al., 2008]. The waveguide support has a refractive index less than of the sample in the cover medium (biological samples typically have refractive indexes in the range of 1.33 to 1.38). The low refractive index in the support is achieved trough the use of nanoporourus silica with a refractive index of 1.2. The reversed symmetry results in a large probing depth into the sample. Waveguides made of silica, with polystyrene waveguiding films with coupling gratings for light coupling have been reported for monitoring of cell growth [Horvath et al., 2008],

but no use of these waveguides for fluorescence microscopy has been reported.

Recently, a symmetrical optical waveguide chip for fluorescence imaging of biological samples has been presented[Agnarsson et al., 2009]. In this case the cladding layer is index-matched to biological samples, and the top cladding layer has a square well that allows for a biological sample. The symmetric geometry of the chip allows for light to be coupled directly into the waveguiding layer of the chip, by coupling light from an optical fiber directly in to the side of the chip. This eliminates the need for any coupling gratings in the waveguiding layer. The penetration depth of the chip can be tuned by varying the chip geometry or core layer material.

In this thesis, the fluorescence imaging properties of such a symmetric waveguide chip have been tested. Procedures for culturing living cells on the chip are described in detail, along with the imaging procedure. The chip has been tested for fluorescence imaging of both fixed and living cells. MCF7 cells were cultured on the chip before being fixed stained with fluorescent markers. The cells have then been imaged with a standard upright microscope. The results for the fixed cells are compared to images of the same cells taken with a standard epi-fluorescence microscope. Living LLC PK1 cells that stably express the fluorescent protein GFP have been used for investigating the possibility of using the chip as a platform for live cell fluorescence imaging. The results from these preliminary tests are presented, along with the adjustments made to accommodate the added demands that are put on the chip to keep the cells alive. The last part of this thesis gives a short description of several integrated optical components that are under development and could further improve the imaging properties of the chip. It also describes how the chip could be an integrated part of a live cell imaging platform.

2 Theory of planar waveguides

By looking at light traveling through a waveguide as rays making the angle ϕ with the axis of the direction of their propagation, the confinement of the light to the waveguiding layer can be explained by the phenomenon of total internal reflection. Light is guided by a dielectric waveguide, like the one illustrated in figure 2.1, provided that the refractive index of the two cladding layers, n_2 is lower than the refractive index of the waveguide core, n_1. When $n_1 > n_2$ the condition for total internal reflection is met, and all light rays traveling through the waveguide in the z-direction, making the angle ϕ with the z-axis that is smaller than or equal to the critical angle $\phi_c = \sin^{-1}(\sqrt{n_1^2 - n_2^2}/n_1)$ will be internally reflected at the core to cladding interface and thereby guided by the waveguide [Okamoto, 2006].

This ray picture of light is a simplified look on the behavior of light, and for a thorough understanding of the behavior of light, it must be regarded as electromagnetic radiation. This chapter covers how Maxwell's equations can be used to derive the equations necessary to mathematically describe the behavior of light guided by the waveguide. These equations are then solved to find the one dimentional distribution of the electrical field in a symmetric waveguide.

2.1 Maxwell's equations

Light is electromagnetic radiation, and can be described by Maxwell's equations, a set of four coupled differential equations. For a homogeneous and lossless dielectric

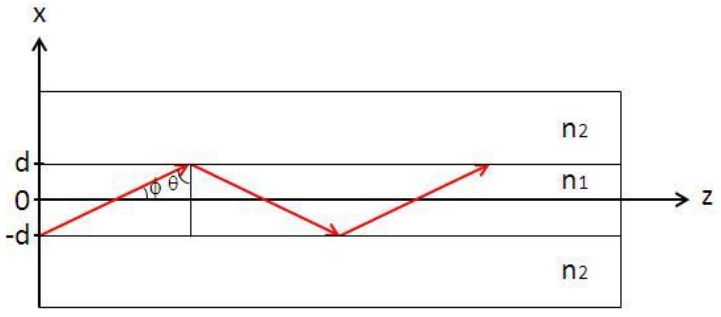

Figure 2.1: Light ray traveling through a symmetric planar waveguide, with core thickness of 2d and a refractive index n_1 in the core and n_2 in the cladding

medium, the Maxwell's equations are [Saleh and Teich, 2007]:

$$\nabla \bullet \mathbf{E} = 0 \tag{2.1}$$

$$\nabla \bullet \mathbf{H} = 0 \tag{2.2}$$

$$\nabla \times \mathbf{E} = -\mu \frac{\partial \mathbf{H}}{\partial t} \tag{2.3}$$

$$\nabla \times \mathbf{H} = \epsilon \frac{\partial \mathbf{E}}{\partial t} \tag{2.4}$$

Where $\mathbf{E}$ is the electric field and $\mathbf{H}$ is the magnetizing field. The parameters ϵ and μ are the permittivity and permeability, respectively, of the medium. These equations, along with the boundary conditions of a system, will describe the behavior of electromagnetic radiation in the system.

2.2 The Helmholtz Equation

By applying a general rule of vectorfields;$\nabla^2 \times (\nabla \times \mathbf{F}) = \nabla(\nabla \bullet \mathbf{F}) - \nabla^2 \mathbf{F}$, to equation (2.3), and using equation (2.4),the wave equation can be derived:

$$\nabla^2 \mathbf{E} - \epsilon\mu \frac{\partial^2 \mathbf{E}}{\partial^2 t} = 0 \tag{2.5}$$

Assuming that the electric field has a harmonic time dependence, $\mathbf{E}(\mathbf{r}, t) = \mathbf{E}(\mathbf{r})e^{-i\omega t}$, which gives $\partial/\partial t \rightarrow -i\omega$, the Helmholtz equation can be derived:

$$\nabla^2 \mathbf{E}(\mathbf{r}) + \epsilon\mu\omega^2 \mathbf{E}(\mathbf{r}) = 0 \tag{2.6}$$

The Helmholts equation holds true for any field or component of an electromagnetic field, and can be written in more general terms:

$$\nabla^2 \mathbf{u} + \gamma^2 \mathbf{u} = 0 \tag{2.7}$$

where $\mathbf{u}$ is any component of the electric or magnetizing fields and $\gamma = \sqrt{\epsilon\mu\omega^2}$. Depending on the medium,γ can be a constant or a function of the position $\mathbf{r}$. For a dielectric material the permittivity and permeability are given by $\varepsilon = \varepsilon_0 n^2$ and $\mu = \mu_0$ respectively. And so for a dielectric medium, γ can be expressed by $\gamma = k^2 n^2$ where k is the wavenumber and n is the refractive index of the medium.

2.3 Finding the E field distribution in 1D for a planar dielectric waveguide

Finding the **E** and **H** field distributions in a planar waveguide is done by solving Maxwell's equations for the specific waveguide. These equations can be solved analytically only in one dimension. We will apply Maxwell's equations to the symmetric planar dielectric waveguide illustrated in figure 2.1, and look for solutions to for electric field profiles in the x-direction. Plane waves traveling through the waveguide in the positive z-direction can be expressed by:

$$\mathbf{E} = \mathbf{E}(x, y)e^{i(\beta z - \omega t)} \tag{2.8}$$

$$\mathbf{H} = \mathbf{H}(x, y)e^{i(\beta z - \omega t)} \tag{2.9}$$

Where β is the propagation constant. The harmonic time dependence gives these expressions of the two curl identities from Maxwell's equations (2.3) and (2.4):

$$\nabla \times \mathbf{E} = i\omega\mu\mathbf{H} \tag{2.10}$$

$$\nabla \times \mathbf{H} = -i\omega\varepsilon\mu\mathbf{E} \tag{2.11}$$

By substituting equations (2.8) and (2.9) into the two curl identities (2.10) and (2.11), the following coupled equations emerge:

$$\frac{\partial E_z}{\partial y} - i\beta E_y = i\omega\mu_0 H_x \tag{2.12}$$

$$i\beta E_x - \frac{\partial E_z}{\partial x} = i\omega\mu_0 H_y \tag{2.13}$$

$$\frac{\partial E_y}{\partial x} - \frac{\partial E_x}{\partial y} = i\omega\mu_o H_z \tag{2.14}$$

$$\frac{\partial H_z}{\partial y} - i\beta H_y = -i\omega\varepsilon E_x \tag{2.15}$$

$$i\beta H_x - \frac{\partial H_z}{\partial x} = -i\omega\varepsilon E_y \tag{2.16}$$

$$\frac{\partial H_y}{\partial x} - \frac{\partial H_x}{\partial y} = -i\omega\varepsilon E_z \tag{2.17}$$

These equations allow for two sets of self-consistent solutions with different polarization properties of the propagating waves. The first three equations represent the transverse electric (TE) mode, where only the electrical field component orthogonal to the plane of incidence is nonzero. The second three represents the transverse

magnetic (TM) mode, where only the magnetic field component orthogonal to the plane of incidence is nonzero. The electrical field components in the two different modes can be derived in a very similar manner, and so only the TE modes are considered here.

In this system, the **E**- and **H**-fields have no y-axis dependence, and so $\partial E/\partial y = \partial H/\partial y = 0$. The three TE-mode equations can be rewritten as:

$$H_x = \frac{\beta}{\omega\mu} E_y \tag{2.18}$$

$$H_z = -\frac{i}{\omega\mu}\frac{dE_y}{dx} \tag{2.19}$$

$$E_x = E_z = H_y = 0 \tag{2.20}$$

These equations relate the two **H**-field components H_x and H_z to the one **E**-field component E_y. The E_y component of the E field can be found by solving the Helmholtz equation. Since $\partial E/\partial y = 0$ and the z-dependence of the field is given by $e^{-i\beta z}$, then $\partial^2/\partial x^2 = -\beta^2$, and the Helmholtz equation for E_y in the TE mode is given by:

$$\frac{d^2E_y}{dx^2} + (k^2n^2 - \beta^2)E_y = 0 \tag{2.21}$$

Light traveling through a waveguide should be confined to the core of the waveguide, and decay exponentially into the cladding. The solution to equation (2.21) can, according to reference [Okamoto, 2006], be written as:

$$E_y = \begin{cases} A\cos(\alpha_1 d - \phi)e^{-\alpha_2(x-d)} & \text{for } x > d \\ A\cos(\alpha_1 x - \phi) & \text{for } -d < x < d \\ A\cos(\alpha_1 d + \phi)e^{\alpha_2(x+d)} & \text{for } x < -d \end{cases}$$

Where:

$$\alpha_1 = \sqrt{k^2n_1^2 - \beta^2} \tag{2.22}$$

$$\alpha_2 = \sqrt{\beta^2 - k^2n_2^2} \tag{2.23}$$

and ϕ is a phase shift. At a dielectric to dielectric boundary, the components of the electric field and the magnetizing field parallel to the interface between the two media must be continous[Saleh and Teich, 2007]. This means that for the symmetric waveguide, the E_y- and H_z-components must be continuous at $x = \pm d$. Since $H_z = -i/\omega\mu dE_y/dx$, the continuity condition for H_z gives that also dE_y/dx must also be

continuous at $x = \pm d$. The dE_y/dx in the three areas can be expressed by:

$$\frac{dE_y}{dx} = \begin{cases} -\alpha_2 A \cos(\alpha_1 d - \phi) e^{-\alpha_2(x-d)} & \text{for } x > d \\ -\alpha_1 A \sin(\alpha_1 x - \phi) & \text{for } -d < x < d \\ \alpha_2 A \cos(\alpha_1 d + \phi) e^{\alpha_2(x+d)} & \text{for } x < -d \end{cases}$$

Here the terms independent of x have been omitted. From the condition that $\frac{dE_y}{dx}$ must be continuous at $\pm d$ these two equations are obtained:

$$\begin{cases} \alpha_2 A/cos(\alpha_1 d - \phi) = \alpha_1 A/sin(\alpha_1 d - \phi) & \text{at } x = d \\ \alpha_2 A/cos(\alpha_1 d + \phi) = \alpha_1 A/sin(\alpha_1 d + \phi) & \text{at } x = -d \end{cases}$$

The constant A can be eliminated, and by calling $\alpha_1 d = u$ og $\alpha_2 d = v$:

$$tan(u + \phi) = \frac{v}{u} \tag{2.24}$$

$$tan(u - \phi) = \frac{v}{u} \tag{2.25}$$

The solution to these two equations can be written as:

$$v = u\, tan(u + \frac{m\pi}{2}) \tag{2.26}$$

$$\phi = \frac{m\pi}{2} \tag{2.27}$$

$m = 0, 1, 2, 3...$

Equation (2.26) is a eigenvalue equation for the TE mode. The value $m = 0$ gives the fundamental mode, while higher order solutions are given by $m > 0$. The parameters u and v are normalized transverse wavenumbers, and they are related by the identity:

$$u^2 + v^2 = k^2 d^2 (n_1^2 - n_2^2) = f^2 \tag{2.28}$$

where f is the normalized frequency. This equation relates u, v and f to the wavelength of the light and the structure of the waveguide.

Equations (2.26) and (2.28) must both hold for a mode to be able to propagate through the waveguide. The allowed modes can be found graphically by plotting $v = u\, tan(u + m\pi/2)$ and $v = \sqrt{f^2 - u^2}$. The point of intersection between the two graphs gives the values of u and v that will propagate trough the waveguide. The parameters u and v are related to the propagation constant β by relation (2.22),(2.23) and:

$$u = \alpha_1 dv = \alpha_2 d \tag{2.29}$$

and so the allowed propagation constants for the E_y field can be found by finding the

intersection between the two graphs. The critical point where higher order modes are cut off is according to reference[Okamoto, 2006] given by $f_c = \pi/2$, and for values of f smaller than f_c, the waveguide is a single mode waveguide.

Another restricting condition for the propagation constant comes from the fact that both α_1 and α_2 must be real for a mode to propagate. This gives the condition that:

$$n_2 < \frac{\beta}{k} < n_1 \tag{2.30}$$

where β/k is a refractive index for the plane wave propagating in the waveguide. It is also called the effective index, n_e, of the propagating mode. When the effective index coincides with the refractive index of the cladding, the mode can not propagate, it will dissipate as a radiation mode. The cut off condition for a mode to propagate is therefore given by:

$$n_{\text{cut off}} = \frac{\beta_{\text{cut off}}}{k} = n_2 \tag{2.31}$$

When $n_e > n_1$ the condition for total internal reflection is not fulfilled, and light is not confined in the waveguiding layer of the waveguide.

Now that the allowed values of β have been found, the only thing missing to completely define E_y in the waveguide, is the constant A. The amplitude A of the E_y-field is determined by specifying the optical power carried by the waveguide. For the TE mode, the optical power P carried by a waveguide is given by [Okamoto, 2006]:

$$P = \frac{\beta}{2\omega\mu_0} \int_{-\infty}^{\infty} |E_y|^2 \, dx \tag{2.32}$$

Substituting the expression for E_y into equation(2.32) gives the following expression for A[Okamoto, 2006]:

$$A = \sqrt{\frac{2\omega\mu_0 P}{\beta d(1 + 1/v)}} \tag{2.33}$$

2.4 The penetration depth

The penetration depth, d, of a bound waveguide mode into the cladding of the waveguide is defined as the distance where the electric field amplitude has dropped to $1/e$ of its value on the interface between the core and the cladding. The electrical field that penetrates into the cladding layer of the waveguide can be expressed by

$E \sim e^{-\alpha_2 x}$, and so the penetration depth is given by:

$$d = \frac{1}{\alpha_2} = \frac{1}{\sqrt{\beta^2 - k^2 n_2^2}} = \frac{\lambda}{2\pi} \frac{1}{\sqrt{n_{\text{eff}}^2 - n_{\text{cladding}}^2}} \tag{2.34}$$

where n_{eff} is the effective index of the waveguide mode. This effective refractive index can be found by numerically solving Maxwell's equations with the boundary conditions imposed by the system. The effective refractive index, and therefore also the penetration depth, is dependent on both the waveguide structure, and the wavelength and polarization of the propagating light.

The intensity of the electric field is proportionate to the square of the electric field amplitude, $I \propto E^2$. At the distance d, the intensity of the field has dropped to $1/e^2$, or about 13%, of its value at the interface between the core and the cladding.

3 Fluorescence microscopy in life science

The average animal cell is about 10 to 20 μm, which is about one fifth of the smallest feature observable by the human eye. So it is clear that optical microscopes are essential tools for the observation of cells and their features. But magnifying the cells is often not enough to study their features, as animal cells are not only too small to observe with the naked eye, they are also both colorless and translucent. To solve this problem a variety of stains that make differnt part of the cell visible have been developed. Some will only bind to fatty acids,other to the mitochondria and so on. They have helped in revealing much about the structure of different cells. Perhaps the most powerful method of staining features of interest in cells is immunostaining; a method that uses antibodies and fluorescent molecules, thereby enabling a very specific binding of fluorescent markers to target molecules in the cells.

3.1 What is fluorescence?

A fluorescent molecule is a molecule that can be excited by a photon and, after a short delay, emits a photon at a longer wavelength.

Three main events govern the process of fluorescence, the first of which is excitation by an incoming photon. The incoming photon has the energy

$$E = hf \tag{3.1}$$

where h is Planck's constant and f the frequency of the photon. If the energy of the incoming photon matches the absorption band of the fluorescent molecule, the molecule is excited from the ground state.

The second event is the vibrational relaxation of the excited state. As the molecule relaxes some of the excitation energy is transformed to molecular vibrations.

The third and last event is the emission of a photon as the molecule returns to its ground state. This photon has lower energy, and therefore a longer wavelength, than the excitatory photon. Depending on the vibrational levels of the ground state and normal thermal motion, a range of emission wavelengths is possible, giving an emission band rather then a single emitted wavelength. The fluorescent molecules make very efficient markers as it is possible, provided that marking is very specific,

to study only the marked parts of a sample by filtering out the excitation signal and only studying the emitted fluorescence signal.

3.1.1 Photobleaching and phototoxicity

A fluorescent molecule can not go through an infinite number of excitation and emission cycles. The average number of cycles for each fluorescent molecule can vary from only emitting a few photons, to thousands or millions of cycles. A molecule in its excited state can react with other molecules and undergo irreversible covalent modifications, thereby losing its fluorescent abilities. When a molecule permanently loses its ability to fluoresce, the molecule is said to be photobleached. Photobleaching presents a problem in fluorescence microscopy as the intensity of the emitted signal drops off over time. The amount of photobleaching is most easily reduced by reducing the exposure of the fluorescent molecules to intense illumination and improving detection sensibility instead.

In living cells photobleaching can also damage the cells. During photobleaching, free radicals can be generated, and oxygen-dependent reactions of these free-radical species causes damage to the cells. The free radicals are said to cause phototoxicity in the cells [Frigault et al., 2009].

3.2 Fluorescence microscopy

The basic idea behind fluorescence microscopy is a very simple one. To study the features of interest in a sample, the features are simply marked with a fluorescent dye. Under the microscope the sample is then illuminated with the excitatory wavelength, and only the emitted signal from the fluorophores is detected and studied.

In reality the picture is, of course, a little bit more complicated. Finding suitable light sources can be challenging, as can filtering away the excitation light from the emitted light since the emitted signal is much weaker. Intense illumination can cause photobleaching, and out of focus fluorescence can cause blurred images.

As a result, many fluorescent microscopy techniques have been developed to optimize the images obtained, and to solve different problems that scientists have encountered. The one thing these methods have in common is that the sample is exposed to light with the excitation wavelength, and that the emitted light is detected. But how this is achieved varies greatly. A few of the most common techniques are mentioned here to show some of the variation in fluorescent microscopy techniques, but also to highlight that there is a niche for the imaging technique presented in this thesis.

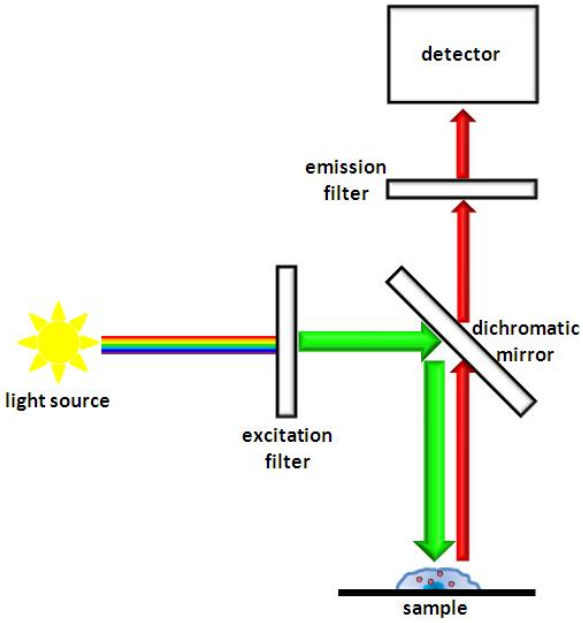

Figure 3.1: A schematic of the basic principle of an epi-fluorescence microscope.

3.2.1 Traditional epi-fluorecence microscope

The epifluorescence microscope is perhaps the simplest fluorescence microscope as it is a normal light microscope with a few additional features that makes it possible to filter out the excitatory light and thereby only detect the fluorescent emission from the specimen.

In these microscopes the sample is illuminated with light that passes through the objective before it thits the sample, in stead of using light that first passes through the specimen. Using this illumination method greatly reduces the amount of excitory light that reaches the objective, as most of the excitory light will pass through the sample, and only a small amount will be reflected back to the objective.

The light source in these microscopes is usually a mercury or xenon arc-discharge lamp. These lamps produce white light with a broad spectrum of wavelengths. As seen in figure 3.1, the light passes through a excitation filter that selects the prefered excitation wavelength. The light is then directed through the objective onto the specimen by a beamsplitter or a dichromatic mirror. The excitatory light excites the fluorophores in the sample, and the emission light from the sample is focused by the objective to the detector. Excitation light is filtered away from the emitted light by a emission filter between the objective and the detector. The image can be viewed directly in the eyepiece or detected by a camera.

In the epifluorescence microscope, the entire sample within the field of view is

illuminated by the excitatory light. This results in the potential excitation of all the fluorescent molecules in this region. This causes problems as fluorescence from the out of focus planes of the sample also will be detected and therefore blur the image. The thicker the sample, the bigger the problem of out of focus fluorescence becomes. The signal to background ratio is low compared to e.g. methods described below.

This method of illumination also presents other challenges. The entire specimen is subjected to quite intense illumination with a relatively broad spectrum, which can cause damage to live cells and tissue, and also causes problems like photobleaching.

The resolution of a microscope is defined as the minimum separation between two points on a specimen that can still be distinguished by the observer or camera system as separate entities. The lateral resolution of a wide-field microscope can be expressed by [Olympus Corporation, 2010]:

$$r_{\mathrm{WF}} = \frac{0.6\lambda}{NA} \tag{3.2}$$

where λ is the emitted wavelengthof the fluorophores and NA is the numerical aperture of the objective.

3.2.2 Total internal reflection fluorescence microscope

The basic idea behind the Total Internal Reflection microscope is to restrict the excitation, and therefore the detection,of fluorophores to a thin region of the specimen. This will eliminate the background fluorescence from outside the focal plane, and the signal-to-background ratio will be dramatically improved. This is achieved by utilizing the well known phenomenon of total internal reflection. A typical setup of a TIRF microscope utilizes the interface between a specimen and a glass coverslip or a plastic tissue culture container. Figure 3.2 illustrates how the incoming light is totally reflected at the interface when the light hits the glass-to-specimen or plastic-to-specimen interface at an angle grater than the critical angle. There will be an evanescent field induced at the boundary that can excite fluorophores in the specimen in a restricted volume adjacent to the interface. The exponential decrease in the away from the interface field restricts the excitation of fluorophores to a region that is typically less then 100 nm in thickness. This eliminates the excitation of fluorophores in the bulk of the specimen, and radically improves the signal to background ratio. The drawback of this technique is that only the part adjacent to the surface can be studied. The short penetration depth of the evanescent field makes the TIRF microscope ideal for the investigation of mechanism and dynamics of cell to cell interactions, detection of single molecules and for events at the cell surface

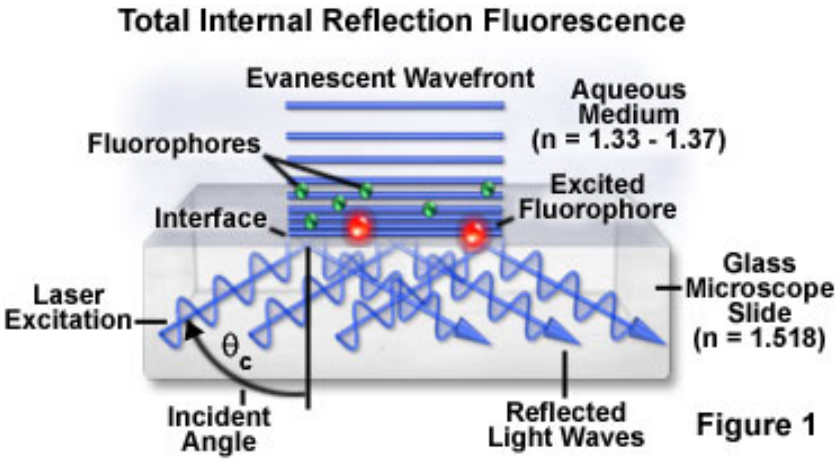

Figure 3.2: A schematic of the basic principle of a TIRF microscope. The evanescent wave induced by total internal reflection at the glass to sample interface excites fluorophores in the sample.Figure from Nikon

or just within the cell membrane, which is a lipid bilayer that is about 5 nm thick [Nikon Instruments, 2010a].

3.2.3 Laser Scanning Confocal microscope

In a laser scanning confocal microscope (LSCM) coherent laser light from the light-source passes through a pinhole aperture. The pinhole is in a conjugate plane with both a scanning point in the sample and a second pinhole aperture placed in front of the detector. This ensures that light focused to a point in the sample is also focused at the second pinhole, and can therefore be detected. Emitted light from fluorophores in out of focus planes in the sample will form Airy disks at the second pinhole, and only a small fraction of the light passes through the pinhole and on to the detector [Claxton et al.]. In this way the out of plane fluorescence is strongly reduced and the signal to background ratio is dramatically improved. The basic principle of a LSCM is illustrated in figure 3.3.

As the microscope can only focus on one point at a time, a complete image of the sample is attained by scanning the sample and a computer is needed to build up a picture from the different datapoints collected by the detector. This scanning can be performed in all three directions, making it possible to attain very good 3D images of the samples. A drawback of this imaging technique is the high intensity and scanning of the sample that makes imaging of live cells difficult.

The lateral resolution of a confocal microscope can be expressed by [Olym-

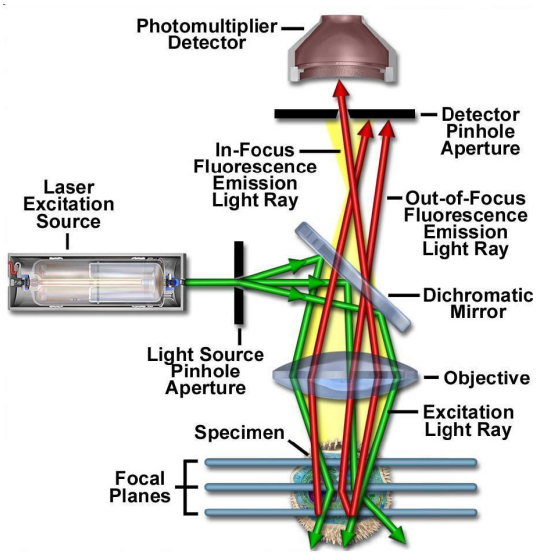

Figure 3.3: A schematic of the basic principle of a confocal microscope. Only light focused on the scanning point of the sample is focused at the detector pinhole aperture, eliminating the detection of out of focus fluorescent emission. Figure from reference [Claxton et al.].

pus Corporation, 2010]:

$$r\text{conf} = \frac{0.4\lambda}{NA} \tag{3.3}$$

Compaired to a wide-field microscope, the confocal microscope has a lateral resolution that is about 30% better. A commonly used equation for the axial resolution of a confocal microscope is given by [Olympus Corporation, 2010]:

$$r_{\text{axial}} = \frac{1.4\lambda n}{NA^2} \tag{3.4}$$

where n is the refractive index of the specimen medium. The axial resolution of a confocal microscope is only marginally improved compaired to that of a wide-field microscope. The advantage of the confocal microscope is the capability of optical sectioning in thick specimens, which results in a dramatic improvement in effective axial resolution over conventional techniques.

4 A symmetric planar waveguide chip for fluorescence microscopy

As discussed in chapter 2, light can be confined to a waveguide core, provided that the core refractive index is higher than the refractive index of the cladding. As the allowed modes propagate through the waveguide, a evanescent field will penetrate a distance d into the two cladding layers. By having a biological sample containing fluorescence labels as part of one of the two cladding layers of the waveguide, this evanescent field can excite fluorophores in the sample that are within the distance of the penetration depth from the waveguide core. This chapter covers the design and basic properties of the symmetrical planar waveguide that has been used for fluorescence microscopy of both fixated and live cells in this thesis.

4.1 The chip

The chip consists of a symmetric planar waveguide on a Si substrate. The two cladding layers are 4 μm thick and are made of the amorphous perfluorinated optical polymer Cytop. This polymer was chosen since it is one of few polymers with a refractive index close to that of both water and cells ($n_{\text{cytop}} = 1.34$), and also for its high optical transmission in the 200 nm to 1600 nm wavelength range and its excellent chemical resistance[Agnarsson et al., 2009]. The chip is fabricated with a square well in the top cladding layer to accommodate for a biological sample. When the well is filled with an aqueous biological sample the top cladding layer will have a relatively uniform refractive index and light traveling through the waveguide will penetrate into the sample without scattering at the edge of the well. The waveguiding layer is made of the polymer PMMA, which was chosen for its relatively high refractive index, $n = 1.49$, and its low autofluorescence [Agnarsson et al., 2009].The thickness of the PMMA layer is of the order of a few hundred nanometers. The basic design of the chip is shown in figure 4.1.

Figure 4.1: The basic design of the symmetric planar waveguide chip, illustrated with two cells in the well.

As mentioned; when light travels through the waveguide, it will penetrate into the aqueous sample in the well. Any fluorescent molecules in the sample that are within the penetration depth from the top of the PMMA layer will be excited. As in the case of TIRF, the limited penetration dept of the excitatory light into the sample will effectively eliminate backgound fluorescence from out of focus areas of the sample. Compared to a epi-fluorescent microscope the chip should therefore be able to produce images with a radically improved signal to background ratio. The penetration depth of the chip is dependent on the waveguide structure, and can therefore be tuned by changing the thickness of the waveguiding PMMA-layer. This enables the production of chips with penetration depths that can be up to several times larger than what is possible with a TIRF microscope[Agnarsson et al., 2009].

4.2 A closer look at the penetration depth

In chapter 2 it was shown that the penetration depth can be calculated using the identity (2.33) The dependence of the penetration depth on the thickness of the PMMA-layer can be found by numerically calculating the effective refractive index of a waveguide with different thickness of the waveguiding layer. This has been done in reference [Agnarsson et al., 2009], and the result is shown figure 7.2. The calculations were performed for the TM mode of 4 wavelengths that are commonly used in fluorescence microscopy. The calculations for n_{eff} were based on a configuration where the top cladding layer had the same refractive index as water. The waveguide is a single mode waveguide up to core thicknesses of approximately 350 nm for blue light, or approximately 500 nm for red light.

For the experimental part of this thesis, cells were grown in the chip well and the well was filled with water during imaging. Water has a refractive index of 1.333, which is close to, but not the same as that of a cell. Cells consist of an outer cell membrane that encloses the cells compartments and the intracellular fluid. The cell membrane is a lipid bilayer that is 3-5 nm thick. This lipid layer can be assumed to have a refractive index of 1.45[Popplewell et al., 2005]. The cytoplasm inside this layer normally has a refractive index of 1.35 to 1.38, and the refractive index is mainly dependent of the protein concentration in the cell [Lianga et al., 2007].

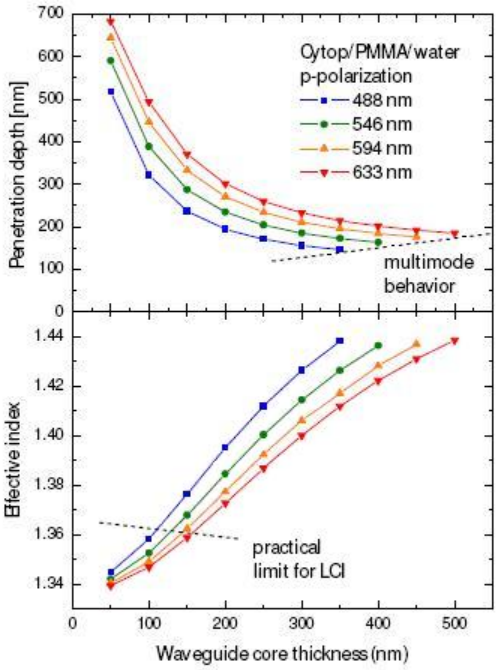

Figure 4.2: Penetration depth of propagating TM polarized light in a PMMA waveguide with a Cytop cladding as a function of waveguide core thickness for four different wavelengths. From reference[Agnarsson et al., 2009]

The impact this slight difference in refractive index will have on the penetration depth of the chip has been estimated by calculating the effective refractive index for a waveguide with fixed PMMA thickness, but with varying refractive index of the top layer. In a 1-D mode solver, a cell as the top cladding layer was modeled as follows: The waveguide structure consisted of a cytop layer as the bottom cladding. A 200 nm thick PMMA layer was the waveguiding layer, and on top of that a cell was modeled by a 4 nm thick lipid bilayer and a layer of cytoplasm with a variable refractive index. The refractive index of the cytoplasm was varied from n=1.333 (for water) up to 1.37. The penetration depth into the cell was then calculated using equation (**??**). Results are shown in figure 4.3 The penetration depth into the sample can vary by tens of nanometers depending on the refractive index of the cells.

4.3 Fabrication

The waveguide chips are fabricated on a 4´´Si wafer. The first step is to spin-coat adhesion promoter (AP3000, DOW Chemical Co.) onto the wafer. The adhesion

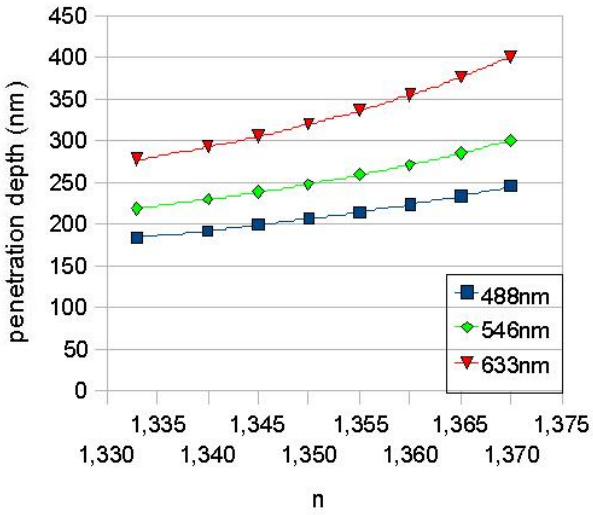

Figure 4.3: The penetration depth of the TE_0 mode as a function of cell refractive index for a waveguide with a 200 nm thick PMMA waveguiding layer.

promoter ensures that a layer of Cytop(approximately 4 μm thick) will adhere to the wafer when spincoated on (figure 4.4b). 25 nm aluminum was then deposited on the Cytop layer [Agnarsson et al., 2010]. Deposition of aluminium on the Cytop surface modifies the surface structure, lowering the contact angle from > 90° to < 90°, and improves adhesion of subsequent layers. The aluminum was removed by wet etching and PMMA spin-coated onto the wafer (figure 4.4 c). A new layer of 200 nm aluminium was deposited, this time to protect PMMA from photoresist solvent (figure 4.4 d). Positive photoresist was spincoated on the aluminium layer (figure 4.4 e) and patterned using standard UV lithography.The wafer was developed, leaving photoresist pads as an etch stop layer covering the well regions on the wafer (figure 4.4 f). A second layer of Cytop was spincoated on (figure 4.4 f). Another 20 nm layer of aluminum was deposited, again to polarize the Cytop layer and enhance the adhesion of subsequent layers. The aluminum layer was then removed. Next a layer of negative photoresist was spin-coated on (figure 4.4 h). Exposure of the negative photoresist patterned it so that the well-areas were exposed after developing the photoresist (figure 4.4 i). Then wells were created by reactive ion etching (figure 4.4 j). To protect the chips, the negative and positive photoresist was left on the wafer as it was diced into individual chips. The remaining photoresist was removed before the chips were used (figure 4.4 k). The chip size was 10 mm x 10 mm with wells of 2 mm x 2 mm, placed in the middle of the chips. Further processing details are given in reference [Agnarsson et al., 2010].

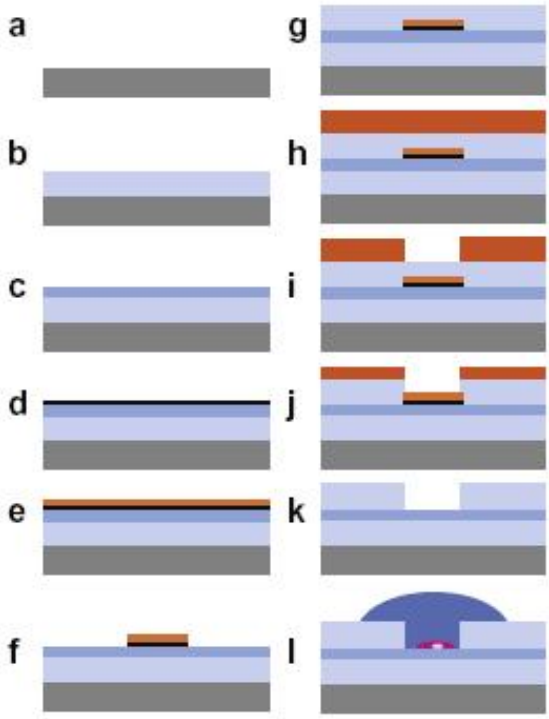

Figure 4.4: Schematic illustration of the main steps in the chip fabrication process from reference [Agnarsson et al., 2010]. Details are given in the text.

5 Imaging of fixed cells

Even though theory indicates that using the waveguide chip for fluorescence microscopy will give pictures with better signal-to-background ratio than a epi-fluorescence microscope, with a much simpler and affordable setup than a TIRF or a LSCM, this must be tested. To examine whether the chip would outperform an epi-fluorescence microscope, cells were seeded on the chips and then fixated and labeled with fluorescent markers. The cells were then imaged, using both an epi-fluorescence microscope and by using evanescent wave excitation. This chapter describes in detail how this was done, and also shows the results of the experiments performed with this setup.

5.1 Cell culture

For the experiments with fixated cells, the Stem Cell Research Unit (SCRU) at the Faculty of Medicine, University of Iceland, kindly provided the breast cancer cell line MCF7, as well as knowledge and facilities for culturing cells.

5.1.1 Cell line

The MCF7 cell line was originally isolated in 1973 by the Ph.D. student Herbert Soule at the Michigan Cancer Foundation [Karmanos Cancer Institute, 2010]. The cells were taken from a woman with metastatic breast carcinoma . They were extracted from a plural effusion discovered during the removal of chest wall nodules. This was the first immortal hormone dependent breast cancer cell line to be extracted, and it is now one of the most commonly used models of estrogen positive breast cancerNugoli et al. [2003]. The MCF7 cell line is an adherent cell line, which means that the cells grow attached to a solid surface, e.g. in a cell culture flask.

5.1.2 Culturing MCF7 cells

The cells were cultured in a 35 ml cell culture flask, in a cell culture medium (CM) Dulbeccos Modified Eagle's Medium (DMEM) supplemented with antibiotics (penicillin and streptividin) and fetal bovine serum (FBS). The culture medium provides the cell with salts, glucose, amino acids and vitamins [Cooper, 2000]. The antibiotics protect the cells from infection. Serum is blood without blood cells and clotting agents, and FBS is blood serum from cow fetuses. The serum is added to the culture media to provide the cells with hormones and growth factors that are

involved in stimulating cell growth and division [Multilab, 2010]. The cells were cultured in an incubator at 37°C with 5% CO_2. The culture medium was refreshed approximately three times a week. The cells were also split up to dilute the cell density, once a week.

5.1.3 Refreshing of culture medium

The cell culture flask was removed from the incubator and put in a sterile fume hood. In the fume hood 5 ml culture medium with 5 % FBS was prepared in a centrifuge tube. Since the MCF7 cells attach to the bottom of the cell culture flask, the old culture medium could be aspirated off the cells from the culture flask with a glass pipette. The new culture medium was then added and the culture flask placed back into the incubator.

5.1.4 Splitting

Before refreshing the culture medium the cells were inspected under a light microscope to estimate the cell density. When the cell density reached approximately 70% to 80% of the culture flask surface, the cells were split.

In the fume hood the culture medium was removed from the cells by the use of a glass pipette. The flask was then rinsed with 5 ml phosphate buffered saline (PBS). When the PBS had been removed, 1ml of 0,25 % Trypsin/EDTA was added to the flask.

Trypsin is an enzyme that cleaves peptide bonds resulting in detachment of the cells from the surface of the culture flask. EDTA is a polyamino carboxylic acid that facilitates the activity of trypsin in this process. It is a chelating agent that binds to calcium, and thereby prevent cadherins from joining. Cadherins are calcium dependent adhesion molecules that bind the cells in a tissue together. Hence adding EDTA to the culture flask will keep the cells from joining together. The culture medium contains components that inhibit trypsin from working properly, and this is the reason for rinsing with PBS. As trypsin works best at 37°C the flask was after this step put in the incubator for 10 minutes. After incubation the flask was put back into the fume hood and 4 ml of PBS is added. The cells should no longer be attached to the culture flask, and any cell clumps could be broken up by pipetting up and down a few times. The 5 ml cell solution was put in a centrifuge tube, and centrifuged at 2000rpm for three minutes. After centrifugation all the cells form a supernatant in the bottom of the tube. This clump contains about $3x10^6$ cells. The fluid is aspirated off, and the cell clump is then dissolved in 1 ml CM containing 5 % FBS. FBS inhibits the activity of Trypsin. 50 μl from this cell solution was then added to an already prepared new cell culture flask containing 5 ml CM with 5% FBS or placed on chips. The new culture flask was then put in the incubator. Only

5 % of the total amount of cells was kept, and within a week they would be ready to be split again. The rest of the cell solution was discarded or used for experiments.

5.1.5 Culturing cells on chips

The MCF7 cells appeared to have no problem attaching to, and growing on, the chip polymer surface of PMMA and Cytop.

Usually cells were plated on six chips at a time. They were placed in a 6-well plate, with one sensor in each well. The chips where first sterilized by UV-light exposure for 10 -15 minutes, before any cells were added. Each sensor was then covered with 3 ml of CM with 5 % FBS. The 6-well plate was then incubated for two days. This gave the cells enough time to attach to the chip surface and to divide.

5.2 Fixing and immunofluorescence staining

Once the chips had been incubated with cells for two days, the amount of cells on the chip surface was high enough to ensure that there would be a suitable number of cells in the well of the chip. For immunofluorescence staining, the chips were removed from the incubator and the cells were fixated and marked with fluorescent markers. Before the detailed acount of the fixation and staining procedure, further information on the use of fluorescent markers will be given.

5.2.1 Immunofluorescence staining

The use of fluorescent labeling enables the researcher to study specific organelles or molecules in a cell. To achieve a very specific recognition of the target molecules, an antibody-based method is used [Alberts et al., 2008].

Antibodies are proteins that are part of the immune systems of vertebrates. They are found in the blood stream and other bodily fluids, and their main task is to recognize foreign objects such as viruses or bacteria. Each antibody recognizes one special target molecule (called a antigen), such as a protein or a polysaccharide on the surface on a foreign object, with a remarkable specificity. This very specific binding between an antibody and its antigen is utilized when samples are stained with fluorescent tags.

Antibodies can be produced for almost any target molecule, and by attaching a small fluorescent molecule to the antibody, one can easily mark the desired parts of a sample with fluorescent tags, as the antibody only binds to its antigen. To amplify the fluorescent signal a method called indirect immunocytochemisty is used. The specific target molecule is first recognized by a primary antibody. This antibody has a very specific affinity to the target molecule. The primary antibody is then

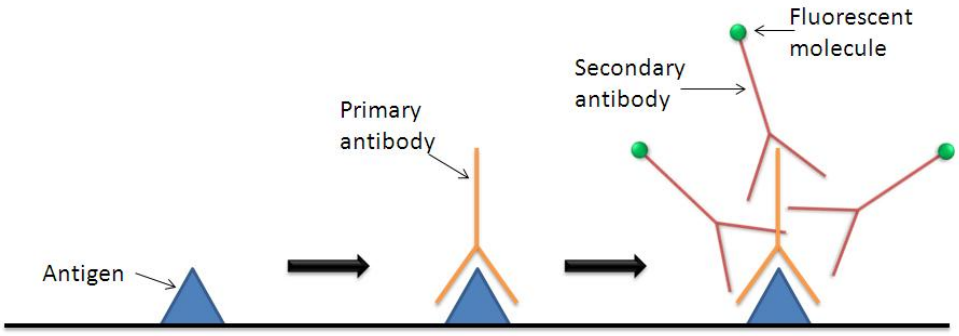

Figure 5.1: The detection of a antigen by primary and secondary antibodies. The primary antibody recognizes the antigen with a very spesiffic affinity. Signal is amplified when several secondary antibodies with fluorescent markers attach to each primary antibody.

recognized by a secondary antibody. The secondary antibodies have fluorescent tags and they recognize the primary antibodies, but not with the same specificity as the primary antibodies. The result is that several secondary antibodies attach to each primary antibody, and the signal is amplified. This is illustrated in figure 5.1.

5.2.2 Fixating and staining of MCF7 cells on chips

Before labeling the cells with fluorophores, the cells were fixated. The fixating ensures that the cells preserve their structure. There are several fixatives available. We have used a paraformaldehyd-Triton fixation. Formaldehyde acts as an cross-linking agent which forms intermolecular bridges that preserves the cell structure. Cross-linking agents, such as formaldehyde, preserves the cell shape better than organic solvents, but they may reduce the access of antibodies to some of the cells compartments, and an extra permeabilizing step is needed in the fixating procedure [IHC-World, 2010].In this procedure the detergent Triton X-100 is used to permeabilize the cells. It does so by solvating the cellular membrane without disturbing any protein-protein interactions [at the University of Illinois at Urbana-Champaign., 2010]. Solvating the cellular membrane ensures the access of the antibodies to the cells and also ensures that the unbound antibodies can be washed out. The more common methanol fixation could not be used on the chips because it caused the polymer layers to delaminate.

The 6-well plate with the chips was taken out of the incubator after two days of incubation. Each chip was removed from the culture medium, placed on a paper towel to remove liquid from underneath, and placed on separate microscope slides. The chips were allowed to dry completely. Since the chips are quite hydrophobic,

one can place a few drops of water on a chip, and the liquid will stay on top of the chip. A hydrophobic marker pen was used to distinguish an area on the microscope slide, around each chip. This ensured that any liquid that spilled of the chip would be contained within this area. The chips were rinsed twice with PBS and subsequently covered with 3.5% formaldehyde for 5 minutes to fix the cells. Cells were then again rinsed twice with PBS before 0.1% Triton X-100 was added, and left for 7 minutes. This step was repeated once, followed up with PBS wash and blocking with 10% FBS/PBS for 10 minutes. Subsequently the chips were incubated with 150 µl of marker-solution containing FBS and the primary antibodies for 30 minutes at room temperature (RT). Afterwards the chips were rinsed thoroughly with PBS and the secondary antibody solution is now added, 150 µl to each chip, and incubated for at least 30 minutes at RT. The chips were again rinsed with PBS, before washing in distilled water. The chip were stored in the dark to avoid photobleaching of the fluorophores.

5.2.3 Proteins stained

The chips used for imaging the fixated cells had a penetration depth of about 200 to 250 nm. Hnce the proteins chosen for marking had to be close to, or within, the cell membrane. Two of the proteins marked are proteins in the cytoskeleton. The cytoskeleton consists of several types of proteins, whose main task is to keep the shape of the cells and to protect the cell from physical stress [Alberts et al., 2008]. One group of these proteins are keratines. Keratines are part of the main filament group of intermediate filaments, and are mainly expressed in epithelial cells. The two cytokeratines that were marked for in the MCF7 cells were keratin 18 and keratin 19. The third protein that was marked is in the surface of the cell membrane. It is an antigen specific for epithelial cells, and has the self-explanatory name of epidermal surface antigen(ESA). The secondary antibodies used had fluorescent molecules with an excitation wavelength of 546 nm and an emission wavelength in the red spectrum.

5.3 Imaging of fixated MCF7 cells

The design of the chip requires the well to be filled with water for the refractive index of the top layer to be more or less uniform, and thereby ensuring that the chip will function as intended. Therefore a drop of water must be sealed under a cover glass before the chip is ready for imaging. This was done by placing a thin black silicone film (PDMS with toner) cut into the shape of a square with a hole in the middle on top of the chip. A drop of deionized water was then placed in the well, and a small piece of cover glass was placed on top. The silicone film sealed the

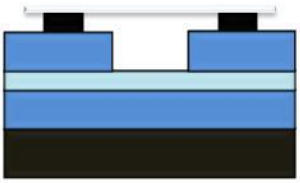

Figure 5.2: The chip with a silicone gasket and coverglass

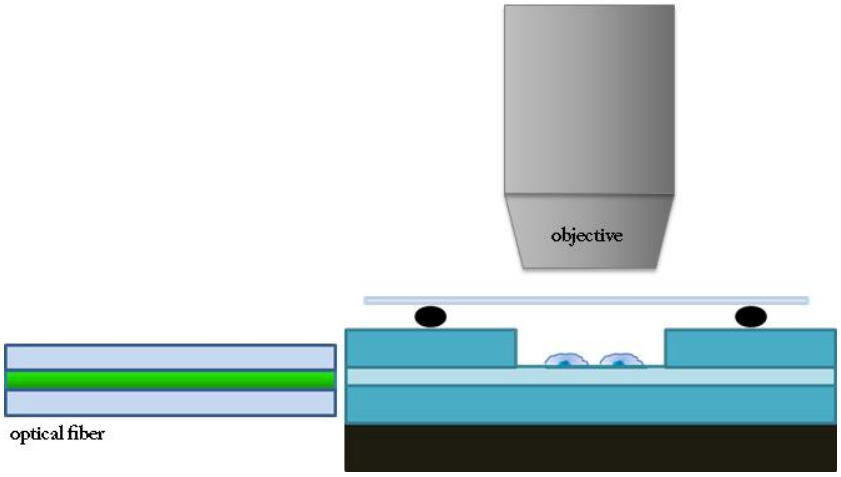

Figure 5.3: A schematic of the imaging set up showing the optical fibre used for light incoupling, a 63x water immersion microscope objective and the sensor with glass cover slip and cells in the well.

water under the cover glass, and the chip was ready for imaging. An illustration can be seen in figure 5.2.

Once prepared, the chip was placed on the microscope stage, and light was coupled into the waveguide. The light source was a SuperK Versa quasi-CW (80MHz) supercontinuum white light source that was coupled in to the chip facet using a optical fiber. An acousto-optical tunable filter attached to the supercontinuum white light source enables the selection of a single or a multiple of up to 8 output wavelengths. The excitation wavelength was carefully tuned to optimize the fluorescent signal from the fluorophores. By choice, all fluorescent molecules used had a excitation wavelength of 546 nm. The emission wavelength of the fluorophores was in the red part of the spectrum.When the exciation light was correctly coupled into the waveguide, only the cells in the well were lit up. A long pass filter was placed in the microscope to filter out the excitation wavelength, so that only the emission of the fluorophores reached the camera. A simple sketch of the imaging setup can be seen in figure 5.3 For successful imaging the output power from the optical fiber

had to be in the range of 100 to 200 μW. The objective used for imaging was a high-resolution 63 x water immersion objective with a numerical aperture of 1.2. For comparison, the chips were also imaged using a traditional epi-fluorescence microscope. The approptiate filters where chosen so that the chip was illuminated with green light. The objective used in this case was a 100x oil immersion lens with a numerical aperture of 1.25.

5.4 Results from imaging of fixated MCF7 cells

The pictures in figures 5.4, 5.5 and 5.6 show fixated MCF7 cells marked for the proteins ESA, keratin18 and keratin19 respectively. The figures also show the epi-fluorecence images taken of the same cells. It is clear that more detail is visible in the chip-images. This is especially evident at the edges of the cells. The signal-to-background ratio is significantly reduced, and the chip therefore produces images in superior quality when it comes to the smaller and less bright details of the parts of the cells adjacent to the surface.

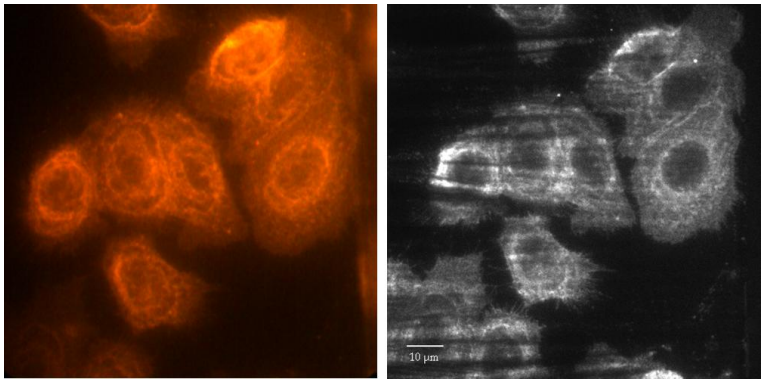

Figure 5.4: Fixed MCF7 cells marked for the cell membrane protein ESA. Left: Image captured with a epi-fluorescence microscope, 100x oil immersion objective with a numerical aperture of 1.25. Right: Image captured using symmetric waveguide excitation, 63x objective with a numerical aperure of 1.2. The size of the scale bar is 10 µm

Even though the chips did produce some very good pictures compared to the epi-fluorescence microscope, the imaging process also revealed some problems with the chip that must be overcome if the chip is going to compete with other techniques. It is evident that the waveguide-excitation can produce dark streaks in the images due to scattering from defects in the waveguide film or from abrupt changes in the refractive index of the sample. Serious examples of these stripes can be seen in figure 5.7. It is possible that streaking effects can be reduced with the use of integrated

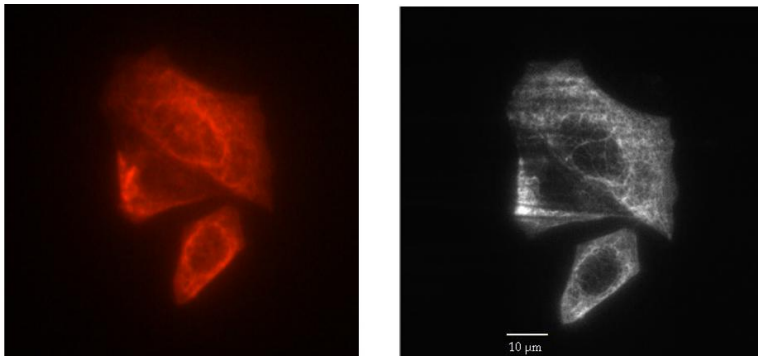

Figure 5.5: Fixed MCF7 cells marked for the cytoskeleton protein keratin 18. Left: Image captured with a epi-fluorescence microscope, 100x oil immersion objective with a numerical aperture of 1.25. Right: Image captured using symmetric waveguide excitation, 63x objective with a numerical aperure of 1.2. The size of the scale bar is 10 µm

optics in the chip, as will be discussed in a later chapter. Also, extreme care, high cleanroom standard and filtered chemicals are required during fabrication.

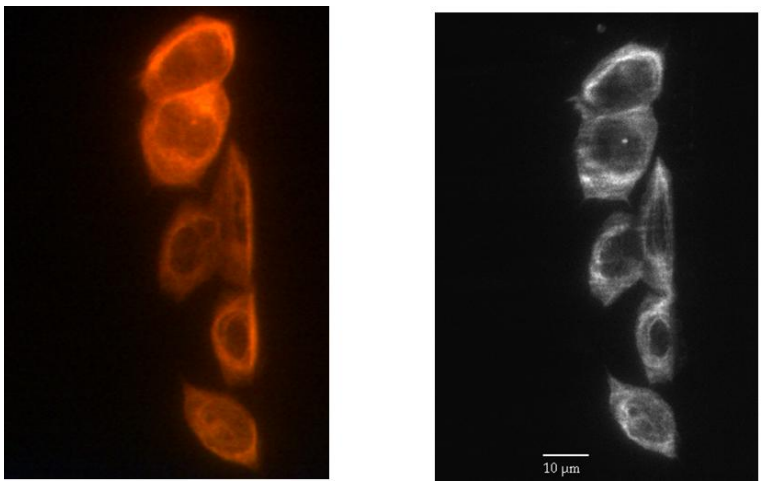

Figure 5.6: Fixed MCF7 cells marked for the cytoskeleton protein keratin 19. Left: Image captured with a epi-fluorescence microscope, 100x oil immersion objective with a numerical aperture of 1.25. Right: Image captured using symmetric waveguide excitation, 63x objective with a numerical aperure of 1.2. The size of the scale bar is 10 µm

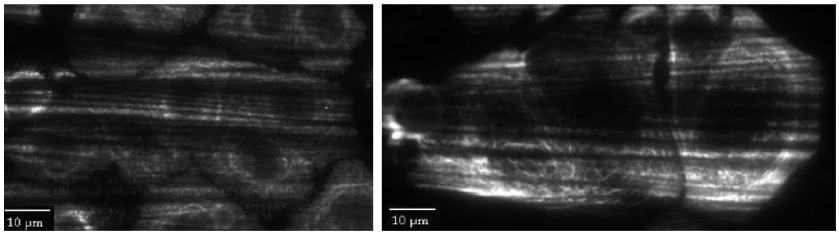

Figure 5.7: Fixed MCF7 cells marked for the cytoskeleton protein cytokeratin 19. Both images were captured using symmetric waveguide excitation with a 63x objective with a numerical aperure of 1.2. The images show examples of the streaking of the waveguide-images that can be caused by scattering from defects in the waveguide film or abrubt changes in refractive index of the sample.

6 Live cell imaging

Imaging of fixed and stained cells can reveal the features of the cells in great detail. These images do, however, only provide a snap-shot of molecular and cellular activity. In addition, the process of fixing the cells before imaging can destroy or disrupt cell components [Alberts et al., 2008]. As a result, imaging of live cells has become a very important tool for scientists to monitor cell activity over time and to make sure that the images acquired provides a correct representation of the cell. This chapter covers the general challenges of live cell imaging, how the chip imaging set up was adapted to meet these challenges, and the result of live cell imaging done with the chip.

6.1 The extra challenges with living cells- in general

Imaging of living cells presents a few challenges compared to imaging of fixed cells. It is mostly a question of keeping the cells as stress-free as possible during the imaging process to avoid imaging stress reactions instead of the normal cell activity. This puts extra requirements both on the microscope system and the environment. Temperature, CO_2 levels, air humidity and light are all factors that can cause stress reactions in the cells, and must be adjusted to the cells needs.

The cells must be kept at a stable level of CO_2 to maintain a stable pH-level. For mammalian cells, an atmosphere of 5% to 10% CO_2 is needed [Frigault et al., 2009]. The cells will not survive for more than a few minutes if the CO_2 gas is removed. To image the cells, they must be removed from the safety of the incubator and placed on the microscope stage. To avoid the cells dying from a lack of CO_2 while under the microscope the cells can be cultured in a complete medium buffered with HEPES to stabilize the pH-level, and the cells will live and profilate for up to 10 hours after CO_2-removal [Frigault et al., 2009]. HEPES is an organic chemical buffering agent that maintains physiological pH despite changes in carbon dioxide concentration. It has no nutritional benefit to the cells [Invitrogen Corporation, 2010]. Another option is to use a culture chamber designed to sustain the cells while under the microscope. These culture chambers are available in a variety of designs, and can provide a stable atmosphere of CO_2 for the cells.

Mammalian cells typically need a constant temperature of 37 °CFrigault et al. [2009]. This results in another requirement for successful live-cell imaging over longer time-intervals; the cells must be maintained at a desired temperature during imaging. This can be done by enclosing the whole microscope in a temperature-controlled box or by a simpler stage top heater. Enclosing the whole microscope

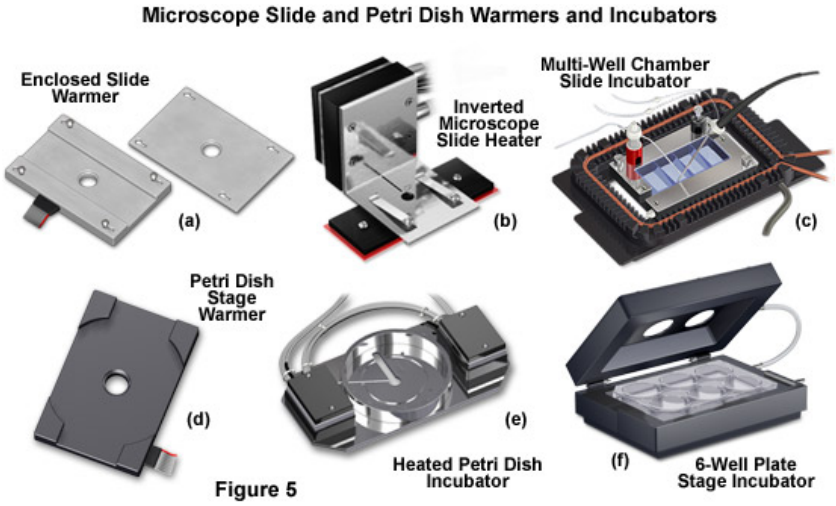

Figure 6.1: A selection of the available designs for stage-top heaters and incubation chambers. Picture from Nikon.

in a temperature-controlled box offer superior temperature stability, but these boxes need a long time to stabilize (> 12 hours [Frigault et al., 2009]), and access to the cells is more difficult. The stage top heater can be a integrated part of a stage top incubation chamber that also provides a stable atmosphere or a simple metal plate designed to fit one type of Petri dish, microscope slide or well-plate. Several designs of stage top heaters and stage top incubation chambers can be seen in figure 6.1. When using an immersion objective it is important to be aware of the fact that the objective will act as a heat sink, and steal heat away from the heating system. This can be avoided by the use of a objective heater [Nikon Instruments, 2010b].

Mammalian cells are sensitive to rapid changes in osmolarity in the culture medium Frigault et al. [2009]. Changes in osmolarity during imaging are caused by evaporation of culture medium. Since most imaging set ups allow for a relative small volume of medium, and the temperature must be kept at 37°C, evaporation of culture medium can be a problem. Most stage top incubators have built in systems to control the humidity in the stage top chamber to avoid evaporation. For simpler solutions, like a Petri dish on a stage top heater, more culture medium must be added to replace the evaporated medium to keep the osmolarity relatively stable, or a closed culture dish can be used.

It should also be mentioned that most cells are not exposed to light during normal life, and so light can both damage and stress the cells. Exposure to UV light can damage the DNA in the cells and IR light can cause heating of the cells. In cells expressing fluorescent proteins, exposure to white light can cause the excitation of fluorophores which can cause both phototoxicity and photobleaching. Keeping the

light exposure of the cells to a minimum is therefore also very important[Frigault et al., 2009].

6.2 Adapting the imaging system to meet the needs of living cells

As mentioned above, live-cell imaging can be quite challenging. Going from imaging of fixed cells to living cells meant that the imaging set up had to be adapted to keep the cells alive during imaging. The first step was to design a small heater, that the chip could rest on during imaging. The heater consists of a piece of plastic with a metal wire that goes through it. On top, a metal plate was placed. The heater is heated by an electrical current passing through the wire. Calibration indicated that a current of 185 mA gives a temperature about 37°Con the surface of a chip placed on top of the heater. The chip was fixed to the heater by double sided tape.

A complete culture medium buffered with HEPES was used to ensure that the cells would not show any stress symptoms because of lack of CO_2 in the atmosphere. Nothing was done to avoid evaporation of culture medium during the imaging process, but more culture medium was added when the amount of culture medium was visibly reduced. Light exposure was minimized by turning the light off in the lab and by blocking the laser light from the optical fiber between image acquisitions.

6.3 Choosing cells for live cell imaging

The immunostaining technique used for MCF7-cells cannot be used to introduce fluorescent molecules into living cells, since part of the process involves fixing, and thereby killing, the cells. Therefore, a cell line that stably expresses fluorescent proteins was needed. Fluorescent molecules occur naturally in some organisms. One of these organisms is the jellyfish Aequorea. The Green Fluorescent Protein (GFP) that naturally occurs in this jellyfish was first discovered by Shimoura et al. in the 1960's [Tsien, 1998]. The gene that encodes GFP has later been both cloned and shown to produce fluorescence when expressed in other organisms [Tsien, 1998]. For the live cell imaging, a cell line that stably expresses GFP was chosen.

The cell line is called LLC PK1, and consists of kidney cells that originate from a Hampshire pig[Hull et al., 1976]. The cells are normal tubular epithelial cells that grow attached to the surface of the cell culture flask. This particular line of LLC PK1 cells has been transfected with a gene that encodes GFP attached to a SH2 domain of a focal adhesion protein. This means that the cell line stably expresses fluorescent proteins that are tagged to the focal adhesion proteins of the

cells. The main task of these focal adhesion proteins is to attach the cells to the surface they grow on. The GFP is also expressed in the nucleus of these cells, but the limited penetration depth of the excitatory light from the waveguide eliminates this from the images. The GFP has an emission wavelength of 509 nm and an excitation wavelength of 488 nm. The expression construct transfected into the cells also contains a sequence that makes the cells resistant to the antibiotic geneticin. This ensures that all cells that express SH2-GFP are also resistant to geneticin, and adding geneticin to the cell culture medium will kill off any cells that are not expressing SH2-GFP.

6.4 Keeping LLC PK1 cells in culture

The cell culture medium used for the LLC PK1 cells was DMEM with 10% FBS and 1% of penicillin-streptomycin (PS). PS is added to avoid bacterial infection. In additon, 100 μg/mL of geneticin was added to the culture medium to kill off any cells not expressing GFP. The cells were incubated at 37 °C in a 5 % CO_2 atmosphere. The culture medium was refreshed and the cells split up approximately twice a week.

6.4.1 Refreshing of culture medium and splitting

The cell culture flask was removed from the incubator and put in a sterile fume-hood. The culture medium was sucked off with a glass pipette before the flask was rinsed twice with 2 ml PBS. The flask was then incubated for 5 minutes with 0.5 ml Trypsin/EDTA in order to free the cells from the surface of the culture flask as described in the previous chapter. After incubation, 4 ml PBS was added to the flask and the liquid was pipetted up and down a few times to break up any cells clumps. The cell solution was then put in a centrifuge glass and centrifuged at 2000 rpm for 3 minutes. After centrifugation, the liquid was sucked out of the centrifuge glass, leaving a clump of cells in the bottom of the glass. The cells were then dissolved in a small amount of culture medium. One third of this solution was added to a new culture flask, and culture medium was added to a total volume of 5 ml in the flask. The new flask was then put in the incubator.

6.5 Preparing chips with live LLC PK1 cells for imaging

Like the MCF7 cells, the LLC PK1 cells had no problem with attaching to, and growing on, the polymer surface of the chips. The main challenges lay in keeping

the cells alive while under the microscope, and finding a method of inducing movement in the cells within the relatively short time span it was possible to keep them alive.

For the first rounds of imaging of live LLC PK1 cells, the cells were incubated on a chip for two days. The cells were grown on the chip in a six well plate using the same procedure as previously described for the MCF7 cell line, with two exceptions: only one chip was incubated at a time, and a larger percentage (50%) of the cell solution was added to the well containing the chip. After two days of incubation, the six well plate with the chip was removed from the incubator and placed in a fume hood. The normal DMEM culture medium was sucked off the chip using a glass pipette and replaced by 3 mL of HEPES buffered phenol-red free medium. The chip with the live cells was then transported to the optics lab while still in the six well plate. In the optics lab, the chip was removed from the culture medium and carefully dried underneath, while making sure that the top surface was not allowed to dry. A silicone gasket and a cover glass was added to the chip in an attempt to seal in the HEPES buffered culture medium to keep it from evaporating. It soon became obvious that the gasket would not stick to the chip surface since the chip could not be dried before attaching the gasket. Instead a drop of culture medium was added to the chip and a coverglass was put on top. This, however, allowed for very little culture medium on top of the cells. The chip with coverglass was put on the heater, and light was coupled in from the side of the waveguide using an optical fiber. The relatively primitive set up kept the cells alive for about an hour, enabling a few image sequences to be aquiered. These image sequences did not, however, reveal any movement of the focal adhesion proteins in the cells. Cells finishing cell division, and therefore attaching and flattening to the surface of the chips were of most interest. The imaging area of the well was small, and few cells were found to be in the finishing stages of cell division at the time of imaging.

To induce some movement in the cells, a second procedure that involved exposing the cells to one of several stress factors was tested. The stress factors included adding epidermal growth factor (EGF) to the culture medium, serum starvation and making a scratch in the cell layer. The three stress factors induce movement in the cells in different ways. EGF has a stimulatory effect on epidermal proliferation, it stimulates the cells to divide [Carpenter and Cohen, 1990]. Cells can be starved by removing the serum (FBS) from the culture medium. Serum starvation is used to synchronize cells in a nondividing state with low metabolic activity [Kues et al., 2000], and reintroducing FBS to the culture medium should regenerate the cell activity. Making a scratch or a wound in the cell layer, induces activity in the focal adhesion proteins as the cells migrate to refill the wound [Liang et al., 2007].

The effect of these three stress factors was tested by culturing LLC PK1 cells in the wells of a six well plate for 48 hours. The stress factors were then introduced

to the cells, and the effect of the stress on the cells was monitored with an epifluorescence microscope. EGF was added to the culture medium at a concentration of 100ng/mL just before imaging. The serum starvation was done by incubating cells for 24 hours, before the culture medium was changed to one that did not have any serum added to it. The cells were then incubated for another 24 hours. Serum was reintroduced to the culture medium just before imaging. To make a wound, a scalpel was used to make a small scratch in the cell layer.

The result of these simple tests showed that adding EFG to the culture medium induced movement in the focal adhesion proteins about an hour after it was added. The serum starvation and scratching the cells did not show the same result, and it was decided to continue only with the EGF to stress cells that were grown on chips.

The imaging of cells stressed by EGF was done by culturing cells on a chip for 48 hours. EGF was then added to the culture medium about an hour before the chip was transported to the optics lab and imaged with the same method used for the "unstressed" cells. This resulted in a time lapse imaging sequence where movement in the focal adhesion proteins is visible.

In addition, a third experiment was set up. The LLC PK1 cells express GFP in their focal adhesion proteins, the main task of which is to attach the cells to the surface they grow on. The idea was to take advantage of this, and image the cells as they attached themselves to the chip surface. Cells were incubated on a chip for about three hours. This allowed the cells to start attaching to the chip surface. The DMEM culture medium was then replaced by a HEPES buffered medium, and the cells were transported to the optics lab. The chip was placed on the heater and a drop of warm (37°C)HEPES buffered medium was added on top of the chip. No coverglass was added, the immersion lens on the microscope was immersed directly into the culture medium covering the chip.

6.6 Imaging of live LLC PK1 cells

Before every imaging session, the heater was put on the microscope stage and coupled to a current source. The heater was pre-heated for at least 30 minutes before the imaging process began. After 30 minutes, the chip was placed on top of the heater, and attached to the heater surface by doublesided tape. Light from a blue laser (473 nm) was coupled into the side of the waveguide using an optical fiber. The output power of the optical fiber was measured to be in the range of 1 mW to 3 mW. This set up kept the cells alive for about an hour. An EM-CCD camera was used to capture the images.

For the first round of imaging, the cells were not exposed to any stress factors other than the imaging itself. Images were obained by a 50x lens with a numerical aperture of 0.70 and can be seen in figure 6.2. In the images one can clearly see

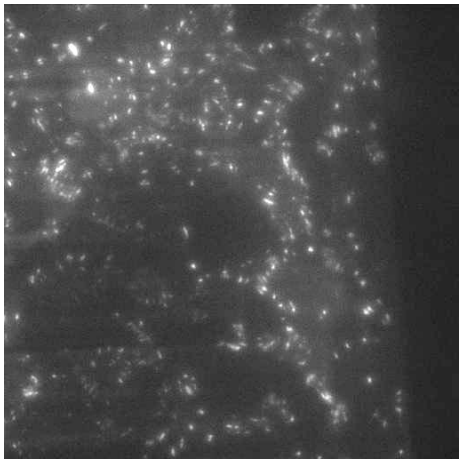

Figure 6.2: Image captured of living LLC PK1 cells showing focal adhesion proteins, using symmetric waveguide excitation and a 63x objective with a numerical aperure of 1.2

the focal adhesion proteins in the cells as small bright dots. For the second round of imaging, stress was induced in the cells by adding EGF to the culture medium an hour before imaging. Images were acquired every 3 minutes over a time span of 30 minutes with a 63x water immersion lens with a numerical aperture of 1.2. This resulted in a time lapse imaging sequence of the cells where one clearly can see movement in the focal adhesion proteins(figure 6.3).

The third round of imaging, this time with cells attaching to the chip, gave an imaging sequence where one clearly can see a cell letting go of the chip surface (figure 6.4). The lens used was a 63 x water immersion lens with a numerical aperture of 1.2

6.7 Comments

Even though the set up proved to be far from ideal to keep cells alive and stress free for time periods longer than an hour, it did provide images of live cells on the chips. The images are of high detail and show little background fluorescence. And by stressing the cells, it was possible to produce time-lapse sequences of the cells that revealed movement in the focal adhesion proteins.

The set up provided good solutions to the problems of CO_2 levels in the atmosphere and light exposure. The HEPES buffered medium held the pH in the cells stable while imaging, and the light exposure of the cells was easily kept at a minimum by turning the laser light off between image acquisitions. The two problem-areas of the set up was temperature-control and presumably also the evaporation of

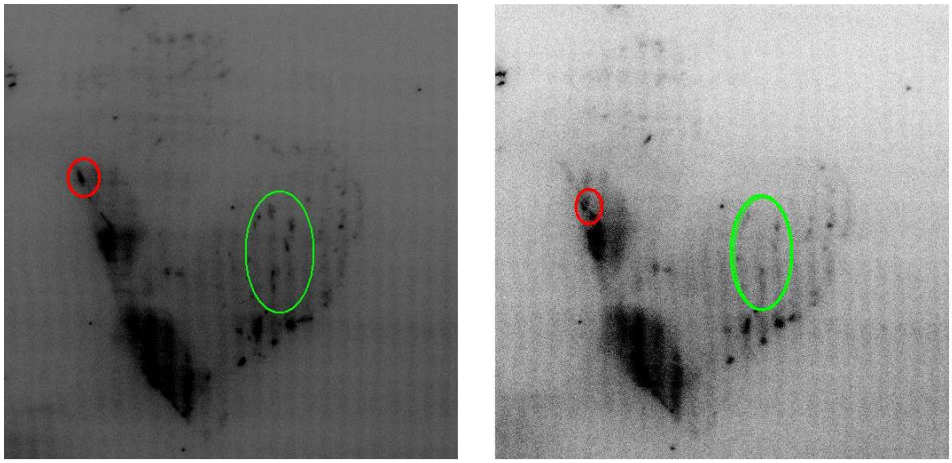

Figure 6.3: Time laps images of living LLC PK1 cells stressed with EGF. Images were obtained using symmetric waveguide excitation and a 63x objective with a numerical aperture of 1.2. The time between the two images is 12.5 minutes. The images have been inverted. The red ring marks an adhesion protein that has moved, the green ring marks an area where several adhesion proteins have detached from the sensor surface.

culture medium. The temperature was not sufficently controlled by the heater, and without any heating of the objective, the immersion lens acted as a heat sink and affected the temperature of the cells. The amount of culture medium that evaporated was not measured, but when the amount was visibly reduced, more culture medium was added. This affected the osmolarity of the culture medium, and did not provide a stable environment for the cells.

The problems of temperature control and culture medium-evaporation can be solved by modifying the chip to allow for a much larger volume of culture medium on top of the chip. With a larger volume of culture medium the effect of evaporation is reduced, and a larger volume of liquid on top of the chip could also help in keeping the temperature more stable. Allowing for a larger volume of culture medium on top of the chip, does, however, mean that it will be very difficult to attain pictures with an upright microscope. A possible solution to this is to make the chip on a glass substrate in order to use a inverted microscope to acquire the images, as is typically done in live cell imaging.

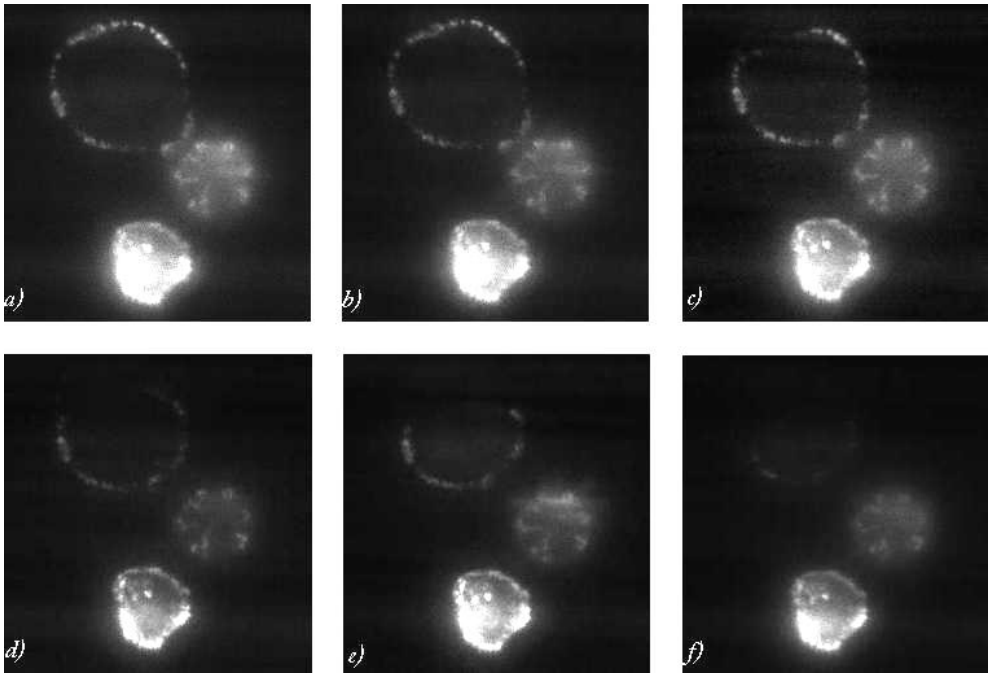

Figure 6.4: Imaging sequence of a LLC PK1 cell detaching from the chip surface. Images were obtained using symmetric waveguide excitation and a 63x objective with a numerical aperure of 1.2. The time between each frame is approximately 3 minutes.

7 Integrated optical components

The chip is capable of high detail imaging, with almost no background fluorescence. It has, however, also shown a few problems of dark streaks in the pictures as a result of scattering from defects in the waveguide film or abrupt changes in the refractive index of the sample. In addition, the live cell imaging revealed a need for better temperature control.

By integrating several optical components to the chip, it is posible to make a integrated optical platform for fluorescence microscopy of biological samples. Optical components like directional couplers, interferometers and ring resonators can be integrated onto the chip and function as beam splitters, thermo-optical switches and temperature measurement devices.

PMMA has proven itself to work very well as the waveguiding layer in the planar waveguide chips. PMMA is also a positive electron beam resist, which means it is possible to pattern single mode channel waveguides and other highly integrated optical components into the PMMA layer by direct e-beam lithography. These components are presently under development [Halldorsson et al., Submitted to Optics Express].

This chapter gives a short introducion to some of these components and how they could be incorporated into a optical platform.

7.1 Channel waveguides

A channel waveguide has the form of a stripe with a finite width. Just as for the planar waveguide, light confinement to the waveguide is dependent on the waveguide having a larger refractive index than the cladding. There is also only a discrete set of modes that can propagate through a channel waveguide, and these modes have evanescent tails that penetrate into the cladding layer. These modes are, however, not as straightforward to derive as the modes for a planar waveguide, and can only be solved numerically.

The mode structure of square cross-sectional channel waveguides can be calculated using the effective index aproximation (EIA). This method calculates the effective refractive index of the propagating modes, and gives a reasonable estimate of the range of single mode operation of the waveguide. Once the effective index is found, the penetration depth of a mode can be calculated using equation (2.33)

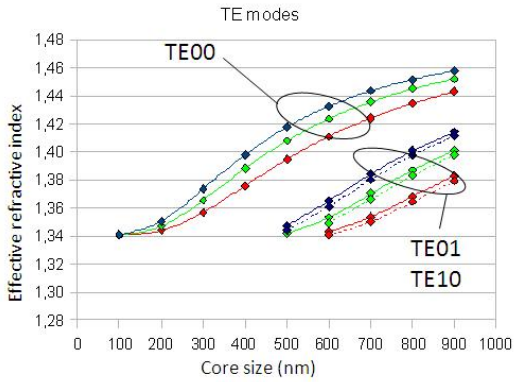

Figure 7.1: The effective refractive index of a PMMA square waveguide in a Cytop cladding for three different wavelenghts as function of core size

given in the theory chapter. This equation is repeated here for convenience:

$$d = \frac{\lambda}{2\pi} \frac{1}{\sqrt{n_{\text{eff}}^2 - n_{\text{cladding}}^2}} \tag{7.1}$$

In a 2D mode solver the effective refractive index of square PMMA waveguides in a uniform Cytop cladding was calculated for three different wavelengths for varying waveguide core size. The result can be seen in figure 7.1.

The calculations displayed in figure 7.1 show that PMMA waveguides in a uninform Cytop cladding will operate as single mode waveguides for the investigated wavelengths for core sizes of 300 nm to 500 nm. The pendetration depth of the TE00 modes for the three wavelengths is displayed as a function of wavelength in figure 7.2

7.1.1 Directional couplers

When two parallel channel waveguides are placed sufficiently close together, the evanescent tails of the propagating modes will overlap, and energy can be transferred from one waveguide to the other by a process of synchronous coherent coupling. The fraction of power that is transferred per unit length depends on the size of the gap between the waveguide channels, the interaction length and the mode penetration into the gap. The coupling length of a directional coupler is defined as the distance for where the power is transferred completely from one waveguide to

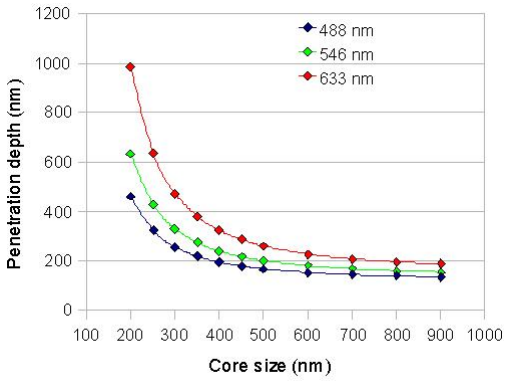

Figure 7.2: The penetration depth of a PMMA square waveguide in a Cytop cladding for varying core size, calculated for three differnt wavelengths.

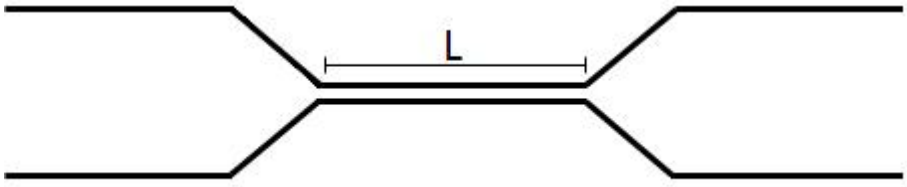

Figure 7.3: A directional coupler of interaction length L

the other. The coupling length is expressed by [Ladouceur and Love, 1996]:

$$L_c = \frac{\lambda}{2\triangle n} = \frac{\lambda}{2(n_{\text{even}} - n_{\text{odd}})} \tag{7.2}$$

Where n_{even} and n_{odd} are the effective refractive index of the even and odd modes in a channel waveguide.

Integrated onto the chip, directional couplers can be used to separate different wavelengths that are propagating in the same channel waveguide. When the interaction length of the coupler is an odd number of coupling lengths for a specific wavelength, light of this wavelength will be totally transferred from one waveguide to the other. For interaction lengths that are a even number of coupling lengths, the light will leave the directional coupler in the same waveguide it entered in. By adjusting both gap size and interaction length, a directional coupler of length $L = L_c(\lambda_1) = 2L_c(\lambda_2)$ will separate λ_1 from λ_2, and the two propagating wavelengths will continue their propagation in separate waveguides.

Some numerical calculations of the effective refractive index of PMMA channel waveguides in a Cytop cladding have been done using the finite element software

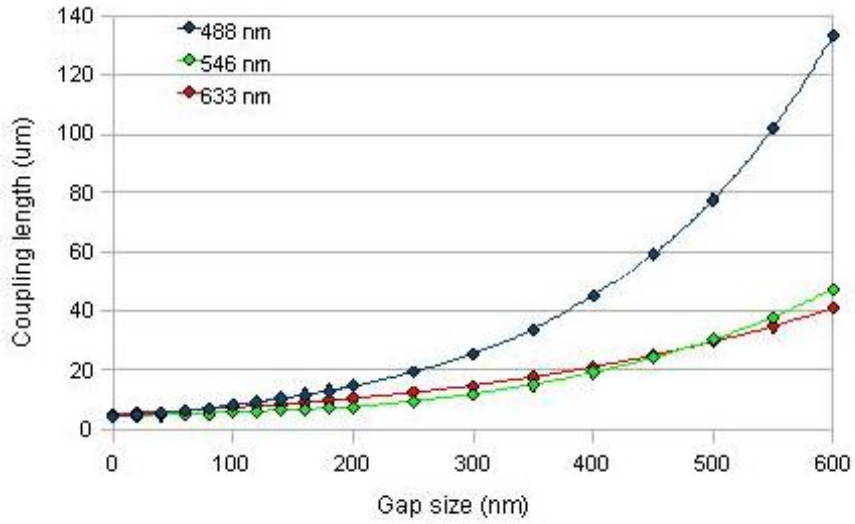

Figure 7.4: The coupling length of a directional coupler as a function of gap size between two 400 nm x 400 nm PMMA square channel waveguides in a Cytop cladding for three different wavelengths of light.

COMSOL. Here the effective refractive index was calculated for waveguides of a fixed size, but with varying gap size and for three different wavelengths. The coupling length was then calculated using equation (7.2). For two 400 nm x 400 nm square PMMA waveguides in a Cytop cladding, the coupling length as function of increasing gap size is shown in figure 7.3 . These calculations can be used to optimize the interaction length and gap size of the coupler to separate two wavelengths over the shortest distance possible.

7.1.2 A thermo-optic switch

Mach-Zehnder Interferometers are commonly used as amplitude modulators or switches[Davis, 2006]. In a Mach-Zehnder interferometer, a channel waveguide is divided into two arms, that are parallel for a distance L, before they are brought together again. By introducing a phaseshift, $\triangle\phi$ for light traveling through one of the two arms, the light will interfere when it will be reunited at the second junction and the output signal is modulated dependent on the phase shift induced. The output intensity, I_{out}, is related to the input intensity, I_{in}, by [Davis, 2006]:

$$\frac{I_{\text{out}}}{I_{\text{in}}} = cos^2\left(\frac{\triangle\phi}{2}\right) \tag{7.3}$$

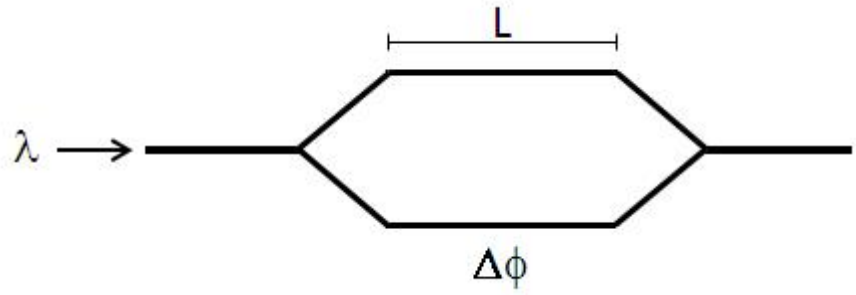

Figure 7.5: A interferometer of length L. A phase shift $\triangle\phi$ is induced between light traveling in the different arms of the interferometer.

for a phaseshift $\triangle\phi$. From equation (7.3) it can be seen that the output intensity will vary from 0% to 100% of the input intensity, depending on the phase shift $\triangle\phi$ provided that the splitting ratio of the y-junction is exactly 50/50.

For the chip, the interferometer could function as an on/off thermo-optical switch by utilizing the fact that all refractive indexes are temperature dependent. From equation (7.3) we see that the interference will result in no output signal when:

$$\triangle\phi = \pi(1 + 2n) \tag{7.4}$$

for $n = 0, 1, 2, 3...$ And by heating one of the interferometer arms the right amount, the effective index of the mode propagating in that arm will change, giving a phase shift that turns turns the signal off. The difference in refractive index, $\triangle n$, between the two arms is related to the phase shift difference and the temperature change $\triangle T$ by:

$$\triangle\phi = \frac{2\pi}{\lambda}\triangle nL \tag{7.5}$$

and

$$\triangle n = \frac{dn}{dT}\triangle T \tag{7.6}$$

where L is the length of the interferometer arms. The heating of one waveguide can be achieved by integrating a thin metal strip above one of the interferometers arms, and the heating can be achieved by passing a current along the metal strip.

7.1.3 Ring resonators

As illustrated in figure 7.6, a ring resonator consists of a circular channel waveguide and one or more straight waveguides that are placed close enough for coupling to occur. Ring resonators have been used in optical communication circuits as wave-

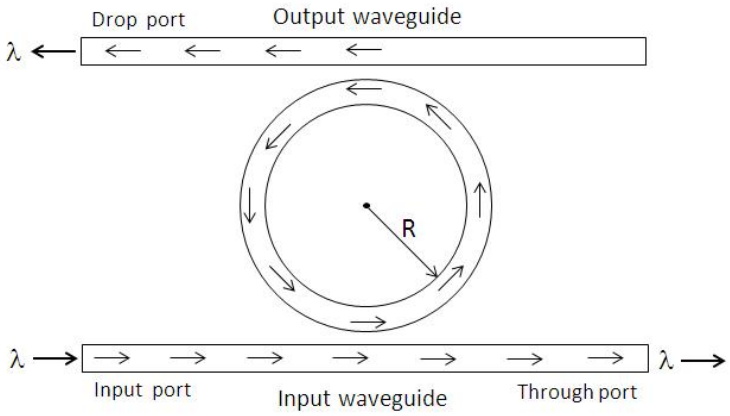

Figure 7.6: A ring resonator of radius R.

length filters, switches and frequency converters[Ramachandrana et al., 2008]. As is the case for the directional couplers, the ring resonator relies on the evanescent tails of the propagating modes to overlap to achieve evanescent field coupling. This enables light to pass from the input waveguide into the ring resonator, and also to pass from the ring to the output waveguide. Constructive interference for light in the resonator ring happens when:

$$2\pi R n_{\text{eff}} = \lambda m \tag{7.7}$$

were m is an integer. A mode that fulfills this condition will interfere constructively within the ring structure. Part of this resonant wavelength escapes the ring into the output waveguide. By controlling the ring parameters, the ring resonator can filter out a specific wavelength from a collection of wavelengths.

The ring resonator is sensitive to changes in refractive index. If n_{eff} changes, the wavelength that will resonate in the ring is shifted. And so the wavelength that will couple out of the ring into the output waveguide is changed. Hence, by monitoring the output at the drop port, one gets information on a changing effective refractive index of the ring resonator. Since refractive indexes are dependent on temperature, the ring resonator can be used to monitor the chip tempereature by monitoring the output signal of the drop port. Temperature control is very important for live cell imaging, and a ring resonator will be able report on the temperature of the chip without interfering with the cells or the setup.

7.2 A waveguide platform for integrated optics

Integration of these kinds of structures onto the chip enables on-chip control over wavelength selection, light switching, wavelength filtering and temperature monitoring. Several wavelengths of light could be coupled in to one waveguide at the edge of the chip. The wavelengths could then be split into separate waveguides by directional couplers. The individual wavelengths could then be switched on and off by thermo-optic interferometers. This enables total control over which wavelengths of light reach the sample well at certain times. Rapid switching between illumination of samples with different wavelengths is also possible. Using channel waveguides to guide the light to the well also enables the waveguide to be split and illuminate the well from two sides or more at the same time. This could eliminate much of the streaking caused by scattering from defects in the waveguide. For live cell imaging, the ring resonator will provide a simple way of monitoring the chip temperature without interfering with the set-up.

8 Conclusion and comments

In this thesis the imaging properties of a symmetric planar waveguide chip have been tested. The waveguide has a cladding that is index matched to that of biological samples, and the top cladding layer has a sample well that accommodates for such samples. Light traveling through the waveguiding layer of the chip penetrates into the cladding and the sample, and any fluorescent molecules in the sample within the distance of the penetration depth of waveguiding layer will be excitied.

The chip has in this thesis been tested for fluorescence imaging of both fixed and living cells. The procedures of culturing cells on the chips have been described in detail, both for the experiments with fixed cells and for the living cells.

For the experiments with fixed cells, cells from the MCF7 cell line were cultured on the chip before being fixed and stained with fluorescent markers. The cells were then imaged using a normal upright light microscope. Light was coupled into the waveguiding layer of the chip using an optical fiber coupled to a light source. For comparison, the cells on the chip were also imaged with a standard epi-fluorescence microscope.

For the experiments with living cells, LLC PK1 cells that stably express the fluorescent protein GFP were cultured on the chip. The imaging set up that was used for the fixed cells was adjusted to accommodate for living cells. Images of the living cells were obtained, and several ways of stressing the cells to induce movement was tested.

The chip has proven to be a useful tool for fluorescence microscopy. The images of fixed cells produced by the waveguiding capabilities of the chip were of very high detail, and showed a significant reduction in the background fluorescence when compared to a standard epi-fluorescence microscope. This is a result of the limited penetration depth of the excitatory light into the sample. The chip makes fluorescence microscopy a possibility on a standard light microscope, and the chip performance is comparable with that of a TIRF microscope. The penetration depth of the light is tunable and can be several times larger than the penetration depth of a TIRF microscope.

The imaging of living cells showed that the chip can be used for live cell fluorescence imaging, even though the imaging setup used did not provide the cells with an optimized environment during imaging. Images of living cells with high detail and almost no background fluorescence were obtained, and some image sequences that showed movement in the adhesion proteins of the cells where obtained by inducing stress reactions in the cells. The chip can therefore be envisioned as an integrated part of a live cell imaging platform. Integrated optical components that

would enhance the imaging properties and the functionality of the chip include directional couplers for splitting of separarte wavelengths, thermo-optic swithces and ring resonators for integrated temperature control.

Bibliography

B. Agnarsson, S. Ingthorsson, T. Gudjonsson, and K. Leosson. Evanescent-wave fluorescence microscopy using symmetric planar waveguides. *Optics Express*, 17:5075–5082, 2009.

B. Agnarsson, J. Halldorsson, N. Arnfinnsdottir, S. Ingthorsson, T. Gudjonsson, and K. Leosson. Fabrication of planar polymer waveguides for evanescent-wave sensing in aqueous environments. *Microelectronic Engineering*, 87:56–61, 2010.

B. Alberts, A. Johnson, J. Lewis, M. Raff, K. Roberts, and P Walter. *Molecular Biology of The Cell*. Garland Science, fifth edition, 2008.

The Imaging Technology Group at the University of Illinois at Urbana-Champaign. Specimen preparation - permeabilization. http://www.itg.uiuc.edu/publications/techreports/99-006/permeabilization.htm, Retrieved April 2010.

D Axelrod. Total internal reflection fluorescence microscopy in cell biology. *Traffic*, 2:764–774, 2001.

G. Carpenter and S. Cohen. Epidermal growth factor. *The Journal of Biological Chemistry*, 265:7709–7712, 1990.

N. S. Claxton, T.J. Fellers, and M.W. Davidson. Laser scanning confocal microscopy. Department of Optical Microscopy and Digital Imaging, National High Magnetic Field Laboratory, The Florida State University.

G.M. Cooper. *The Cell - a molecular approach*. Sinauer Associates, Inc., second edition, 2000.

Christopher C. Davis. *Lasers and Electro-optics, Fundamentals and Engineering*. Cambridge University Press, fourth edition, 2006.

M. M. Frigault, J. Lacoste, Swift J. L., and C. M. Brown. Live-cell microscopy - tips and tools. *Journal of Cell Science*, 122:753–767, 2009.

H.M. Grandin, B. Stadler, M. Textor, and J. Voros. Waveguide excitation fluorescence microscopy: A new tool for sensing and imaging the biointerface. *Biosensors and Bioelectronics*, 21:1476–1482, 2006.

J. Halldorsson, N. Arnfinnsdottir, A. Jonsdottir, B. Agnarsson, and K. Leosson. High index contrast polymer waveguide platform for integrated biophotonics. *Optics Express*, Submitted to Optics Express.

R. Horvath, K. Cottier, H.C. Pedersen, and Jeremy J. Ramsden. Multidepth screening of living cells using optical waveguides. *Biosensors and Bioelectronics*, 24: 799–804, 2008.

R. N. Hull, W. R. Cherry, and W. Weaver. The origin and charachteristics of a pig kidney cell strain, llc-pk$_1$. *In Vitro*, 12:670–677, 1976.

IHC-World. Immunocytochemistry methods, techniques and protocols. http://www.ihcworld.com/_protocols/general_ICC/fixation.htm, Retrieved April 2010.

The Invitrogen Corporation. Cell culture reagents. http://www.invitrogen.com/site/us/en/home/Products-and-Services/Applications/Cell-Culture/Mammalian-Cell-Culture/reagents/hepes.html, Retrieved April 2010.

The Karmanos Cancer Institute. History of achievements - fighting cancer for more than 60 years. http://www.karmanos.org/app.asp?id=13&ssec=1, Retrieved March 2010.

M. Kues, W.A.and Anger, J.W. Carnwath, D. Paul, J. Motlik, and H. Niemann. Cell cycle synchronization of porcine fetal fibroblasts: Effects of serum deprivation and reversible cell cycle inhibitors. *Biology of Reproduction*, 62:412–419, 2000.

F. Ladouceur and J.D. Love. *Silica-Based Buried Channel Waveguides and Devices*. Chapman & Hall, 1996.

C. Liang, A.Y. Park, and J. Guan. In vitro scratch assay: a convenient and inexpensive method for analysis of cell migration in vitro. *Nature Protocols*, 2:329–333, 2007.

X.J. Lianga, A.Q. Liua, C.S. Limb, T.C. Ayic, and P.H. Yap. Determining refractive index of single living cell using an integrated microchip. *Sensors and Actuators A*, 133:349–354, 2007.

Multilab. Functions of serum in the culture medium. http://www.molecular-plant-biotechnology.info/animal-tissue-culture-and-hybridoma-technology/functions-of-serum-in-the-culture-medium.htm, Retrieved April 2010.

Inc. Nikon Instruments. Introduction to fluorescence microscopy. http://www.microscopyu.com/articles/fluorescence/fluorescenceintro.html, Retrieved March 2010a.

Inc. Nikon Instruments. Maintaining live cells on the microscope stage. http://www.microscopyu.com/articles/livecellimaging/livecellmaintenance.html, Retrieved March 2010b.

M. Nugoli, P. Chuchana, J. Vendrell, B. Orsetti, L. Ursule, C. Nguyen, D. Birnbaum, E. Douzery, P. Cohen, and C. Theillet. Genetic variability in mcf-7 sublines: evidence of rapid genomic and rna expression profile modifications. *BMC cancer*, 3:13, 2003.

Katsunari Okamoto. *Fundamentals of Optical Waveguides*. Elsevier, second edition, 2006.

The Olympus Corporation. Resolution and contrast in confocal microscopy. http://www.olympusfluoview.com/theory/resolutionintro.html, Retrieved May 2010.

J. Popplewell, N. Freeman, S. Carrington, G. Ronan, C McDonnell, and R.C. Ford. Quantitfication of the effects of melittin on liposome structure. *Biochemical Society Transactions*, 33:931–933, 2005.

A. Ramachandrana, S. Wang, J. Clarke, S.J Jaa, D. Goada, E.M. Walda, L.and Flooda, E. Knobbea, J.V . Hryniewicz, S.T. Chu, D. Gill, W. Chen, O. King, and Little B.E. A universal biosensing platform based on optical micro-ring resonators. *Biosensors and Bioelectronics*, 23:939–944, 2008.

B. E. A. Saleh and M. C. Teich. *Fundamentals of photonics*. Wiley, second edition, 2007.

R.Y. Tsien. The green fluorescent protein. *Annual Review of Biochemistry*, 67: 509–544, 1998.